


# Optical Microscopy Systems for the Detection of Unlabeled Nanoparticles

Ralf P Friedrich<sup>1</sup>, Mona Kappes<sup>1</sup>, Iwona Cicha<sup>1</sup>, Rainer Tietze<sup>1</sup>, Christian Braun<sup>2</sup>, Regine Schneider-Stock<sup>3</sup>, Roland Nagy<sup>4</sup>, Christoph Alexiou<sup>1</sup>, Christina Janko<sup>1</sup> 

<sup>1</sup>Department of Otorhinolaryngology, Head and Neck Surgery, Section of Experimental Oncology and Nanomedicine (SEON), Else Kröner-Fresenius-Stiftung Professorship, Universitätsklinikum Erlangen, Erlangen, 91054, Germany; <sup>2</sup>Institute of Legal Medicine, Ludwig-Maximilians-Universität München, München, 80336, Germany; <sup>3</sup>Experimental Tumor Pathology, Institute of Pathology, University Hospital, Friedrich-Alexander-Universität Erlangen-Nürnberg, Erlangen, 91054, Germany; <sup>4</sup>Department Elektrotechnik-Elektronik-Informationstechnik (EEI), Friedrich-Alexander-Universität Erlangen-Nürnberg, Erlangen, 91058, Germany

Correspondence: Christina Janko, Department of Otorhinolaryngology, Head and Neck Surgery, Section of Experimental Oncology and Nanomedicine (SEON), Else Kröner-Fresenius-Stiftung Professorship, Universitätsklinikum Erlangen, Glückstrasse 10a, Erlangen, 91054, Germany, Tel +49 9131 85 33142, Fax +49 9131 85 34808, Email christina.janko@uk-erlangen.de

**Abstract:** Label-free detection of nanoparticles is essential for a thorough evaluation of their cellular effects. In particular, nanoparticles intended for medical applications must be carefully analyzed in terms of their interactions with cells, tissues, and organs. Since the labeling causes a strong change in the physicochemical properties and thus also alters the interactions of the particles with the surrounding tissue, the use of fluorescently labeled particles is inadequate to characterize the effects of unlabeled particles. Further, labeling may affect cellular uptake and biocompatibility of nanoparticles. Thus, label-free techniques have been recently developed and implemented to ensure a reliable characterization of nanoparticles.

This review provides an overview of frequently used label-free visualization techniques and highlights recent studies on the development and usage of microscopy systems based on reflectance, darkfield, differential interference contrast, optical coherence, photothermal, holographic, photoacoustic, total internal reflection, surface plasmon resonance, Rayleigh light scattering, hyperspectral and reflectance structured illumination imaging. Using these imaging modalities, there is a strong enhancement in the reliability of experiments concerning cellular uptake and biocompatibility of nanoparticles, which is crucial for preclinical evaluations and future medical applications.

**Keywords:** label free imaging, nanoparticle detection, non-fluorescent imaging, reflectance imaging, holotomography, scattering microscopy

## Introduction

Nanoparticles (NPs) play an increasingly important role in the development of therapeutics and diagnostic contrast agents. In particular, iron oxide nanoparticles, due to their magnetic properties, enable some innovative therapeutic approaches, including magnetic drug targeting (MDT) or hyperthermia, for the treatment of various diseases such as cancer. Furthermore, they serve as contrast agents for magnetic resonance imaging (MRI), and in stem cell therapy for monitoring, targeted delivery or triggering a desired cell differentiation.<sup>1–5</sup> Apart from iron oxide NPs, also non-magnetic metallic or organic NPs play a prominent role in nanoparticle-based therapies or/and as contrast agents.<sup>6–8</sup> In addition to the particle size and shape, the surface chemistry determines the utility of the particles, as it is responsible for the interactions with the environment.<sup>9</sup> Even small changes in size, charge, hydrophobicity, etc. can lead to a significant alteration in the adsorption of biomolecules and corona formation, as well as to a shift in stability, internalization, biocompatibility or biological effect of the NPs.<sup>1,10–12</sup> From this point of view, the characterization and validation of the developed particle systems should be conducted without any additional modification of the particle surface. This applies not only to the required toxicity measurements, but also to the investigation of cellular binding and uptake.

Currently, there are several methods suitable for the detection and quantification of unlabeled NPs.<sup>13–16</sup> However, most of those techniques, such as MRI, positron emission tomography (PET), ultraviolet spectrophotometry (UVS), magnetic resonance ((1)H-NMR) spectroscopy and magnetorelaxometry (MRX), are not applicable for determination of the cellular localization.<sup>15,17–20</sup> In contrast to those methods, transmission electron microscopy (TEM), due to its extremely high resolution, is able to very clearly visualize the amount and localization of nanoparticles and their interaction with cellular structures.<sup>21–23</sup> This also applies to fluorescence-based confocal microscopy and related high-resolution optical microscopy systems such as super-resolution confocal live imaging microscopy (SCLIM), stimulated emission depletion microscopy (STED), photoactivated localization microscopy (PALM), structured illumination microscopy (SIM) and stochastic optical resolution microscopy (STORM) with which, in contrast to TEM, the observation of structures within living cells is feasible.<sup>24–26</sup> However, optical microscopy usually requires fluorescent labeling to visualize cellular compartments or other structures. Thus, observation and characterization of structures, such as molecules, proteins or nanomaterials requires a prior labeling with fluorescent dyes, which can significantly alter the particle properties, thus permitting limited information on biocompatibility and other cellular effects.<sup>27,28</sup>

To eliminate these drawbacks, several other optical and spectral methods are now available that allow investigations of cellular localization and activity of label-free nanoparticles (Figure 1).<sup>29,30</sup> These techniques include hyperspectral dark-field and bright-field microscopy, which records the spatial and spectral information of each pixel to produce a 3-dimensional spectral image, or holotomographic microscopy, a laser technique which produces a three-dimensional refractive index (RI) tomogram.<sup>31–33</sup>

Confocal reflectance imaging (CRM) is another imaging technique based on the detection of light backscattered from reflective objects and can therefore be used without further labeling with fluorescent markers. Reflectance-based imaging can be accomplished with many microscopic systems by adding a transmission/reflection dichroic, which facilitates the collection of reflected incident light. Moreover, the combination with fluorescence imaging provides additional visualization about cellular components.<sup>34</sup> In addition, CRM allows acquisition of high-resolution images with increased spatial resolution and has been used for many years in clinics and preclinical research to visualize morphologic changes in skin lesions and diseases, as well as cytopathic effects of cutaneous parasites, fungi, bacteria, and viruses.<sup>35,36</sup> However, this technique can also be used to examine other areas of the body, such as various tissues in the head and neck, as well as for frozen section analyses, in order to visualize cytological features without the artifacts of histologic processing.<sup>37</sup> The information obtained from CRM can thus lead to a more accurate diagnosis and ultimately a successful treatment strategy without the need for invasive biopsies. In addition to the use of CRM in dermatology, other research areas addressing cellular changes after exposure to agents or nanomaterials can also benefit from this technique. In principle, reflected or scattering light can be processed in a variety of different optical microscopy systems, including confocal systems, to obtain additional parameters about eg nanomaterials, which are becoming increasingly important in research and clinical applications.<sup>38</sup> The detection systems are all based on the generation of a reflectance or scattering image resulting from RI changes, which are the greatest source of contrast in confocal images of microscopic tissue structures.<sup>39</sup> As a result, visualization of unlabeled structures is enabled, which is particularly necessary in medical research, for thorough assessment of cellular particle uptake and localization, to enable more reliable predictions of NP biocompatibility and mode of action. As such, non-fluorescent optical microscopy can either confirm the results of fluorescence-based studies, complement the data with additional structural information, or refute the results obtained with fluorescently labeled samples due to labeling-related alterations of NP properties.

This review describes several frequently used optical microscopy systems and highlights recent reports addressing characterization, detection or impact of label-free NPs using those modalities.

## Imaging Techniques

### Confocal Reflectance Microscopy (CRM)

Confocal microscopy relies on a conjugate pinhole system to block out unfocused light in order to collect light from only one plane. Compared to epi-illumination, this results in a significant improvement in resolution and contrast, thus enabling three-dimensional (3D) confocal imaging with optical sections through biological samples. For the detection of reflection instead of fluorescence light, only a transmission/reflection dichroic needs to be added to the confocal system

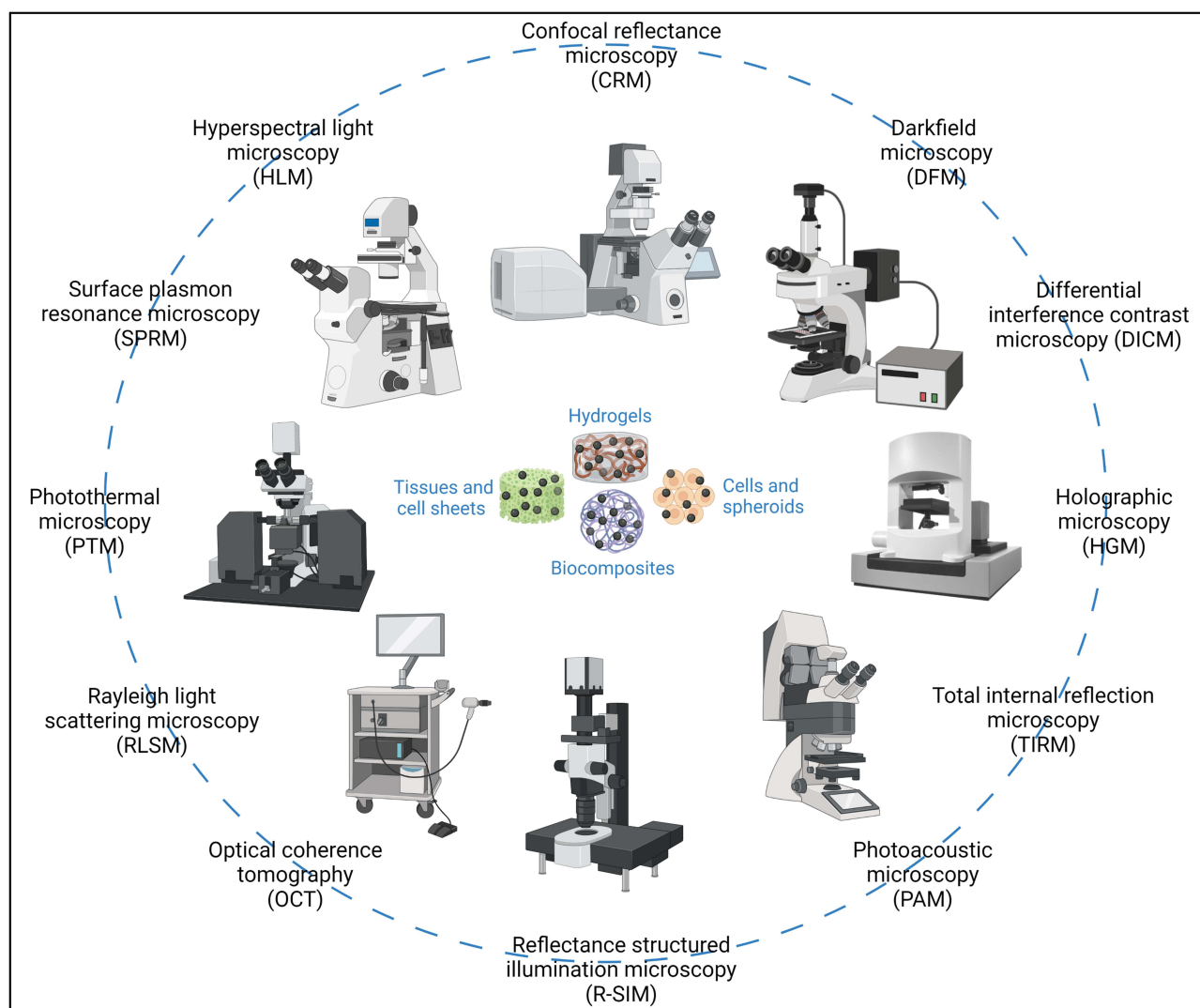


**Figure 1** Selection of microscopy systems which are capable of or can be modified for reflectance- or scattering-based localization of label-free nanoparticles (The pictures are merely intended to illustrate the large number of possible microscopy systems and are not supposed to represent an explicit microscope type or manufacturer). (Image created with BioRender.com).

to enable CRM imaging, where the reflection alone or in combination with the fluorescence signal of a sample can be imaged.<sup>38</sup> However, direct fluorescence labeling is not mandatory as long as the sample structures show sufficient contrast. This applies to all samples and tissues containing high contrast structures, and even more so to NPs made of metals or metal oxides. Thus, CRM can be used for many applications, such as diagnosis of accessible tissue surfaces, detection and monitoring of NPs in regenerative medicine, verifying the presence and biodistribution of NPs in biological samples, and evaluating the short- and long-term toxicity of NPs.

### CRM for Diagnostics

CRM is a widely used tool to obtain functional and morphological information about cells and tissues.<sup>40</sup> Moreover, CRM on live human skin has been long used by dermatologists as a rapid and non-invasive diagnostic tool to image high-contrast optical “slices” of normal and altered skin that correlates well with histologic results.<sup>41,42</sup> In a study by Maitland et al, a fiber optic confocal reflectance microscopy (F-CRM) enabled discrimination between normal and neoplastic tissue of the oral mucosa and demonstrated the clinical potential of F-CRM as a sensitive and specific method for non-invasive detection of precancerous and cancerous lesions in the oral cavity.<sup>43</sup> However, the use of F-CRM is not limited to the analysis of the skin, as it also allows in vivo examination of mucosae and even inner organs. Ando et al used

a flexible fiber optic device that allows imaging of the brain and other organs. By combining bioluminescence imaging (BLI) of luciferase reporter mice with reflectance imaging, they correlated the structural details of the bioluminescence images with the distinct structures of blood vessels and organs visualized by reflectance.<sup>44</sup>

### CRM for Label-Free NP Detection

CRM can also be used to study NP exposure and uptake using appropriate *in vitro* models, for example based on epidermal keratinocytes. Similarly, it allows easy and reliable examination of the effects of direct interactions between NPs and skin, which is very important for the development of drug delivery applications and their monitoring.<sup>40</sup> CRM can also be used for the diagnosis of diseases that may arise as a result of nanoparticle exposure. For example, cutaneous chrysiasis, which may develop following parenteral administration or topical exposure to gold-containing substances or materials, can be detected by CRM as hyperreflective subcellular particles in the dermis and confirmed by histopathological analysis, dark-field illumination with hyperspectral imaging, and neutron activation analysis.<sup>45</sup> CRM-based detection of NP uptake is also possible in whole animals, eg in the aquatic model organism *Daphnia Magna*, thus providing the opportunity to study the effects of NP exposure in living organisms.<sup>46</sup>

Silver nanoparticles (AgNPs) are widely used as biocides in consumer products and medical devices and, depending on the dose, can cause serious disorders in various organisms, including humans.<sup>47</sup> In the work of Tardillo Suárez et al, the effects and subcellular distribution of AgNPs and Ag (I) species were studied *in vitro* after AgNP-exposure of hepatic cells using several high-resolution imaging techniques, including CRM.<sup>48</sup> They identified the transport of AgNP-containing lysosomes to a perinuclear site and a nuclear transfer of Ag (I) species with accumulation in the nucleoli. Even at very low dosages, nuclear receptors, such as liver X receptor (LXR) and farnesoid X receptor (FXR), were inhibited and, consequently, could induce adverse endocrinological effects.

The uptake of particles and their intracellular transport is also of great interest in the drug delivery research and toxicology-related investigations, as it has a major impact on many biological processes. For instance, following optical detection of particles in vital cells by CRM and dark-field microscopy, Wagner et al presented a method for automatic classification and segmentation of particle trajectories suitable for various types of single-particle tracking experiments.<sup>49,50</sup> Our own studies often focus on the cellular uptake of nanoparticles and their cellular effects. For this reason, we used confocal reflectance microscopy to demonstrate whether poly (acrylic acid-co-maleic acid)-coated superparamagnetic iron oxide nanoparticles (SPION<sup>PAM</sup>, which are suitable eg for magnetic labeling of cells, tissue engineering and functionalization with biologically active substances), are actually taken up by cells or merely adhere to the cell membrane.<sup>51–53</sup> After 24 h incubation with SPION<sup>PAM</sup> at 2 µg per mL cell culture medium, followed by staining of cells with a cytoskeleton (phalloidin Alexa 488) and nuclear marker (Hoechst), cells were examined with CRM (Figures 2, 3 and [Supplemental Material](#)). The images confirmed a strong perinuclear concentration of single particle agglomerates (Figures 2A–E), which appeared much more detailed under reflectance mode than under transmitted light (Figure 2D vs C). Imaging of multiple Z-stacks and the resulting 3-dimensional images, as well as videos, confirmed the incorporation of particles (Figure 2F, G, and [Supplementary Video 1](#)). The high-resolution details of the CRM system of individual particle clusters were successfully visualized at a high magnification of a single image (Figure 3A and B). The intensity profile of a line drawn through several objects shows a half-width maximum of about 214 nm, which is approximately the size of SPION<sup>PAM</sup> (180 nm) (Figure 3C).<sup>51</sup> Accordingly, single large particles can be well visualized with CRM, provided they are not too close together or form agglomerates.

### Molecular Confocal Reflectance Microscopy (M-CRM)

Apart from enabling imaging of unlabeled NPs, optical reflectance-based methods can also serve for precise imaging of target biomolecules. In order to deliver satisfactory results, the contrast differences between cellular structures and their surroundings must be sufficiently high. This problem can be resolved by the use of molecular contrast probes consisting of NPs coupled with specific catcher proteins or antibodies. For example, Sokolov et al demonstrated that CRM is suitable for molecular imaging of cell suspensions, three-dimensional cell cultures, and fresh cervical biopsies.<sup>54</sup> After local administration of bioconjugates containing gold nanoparticles (AuNPs) and probe molecules for specific cellular biomarkers, such as antibodies against epidermal growth factor receptor (EGFR) overexpressed in epithelial



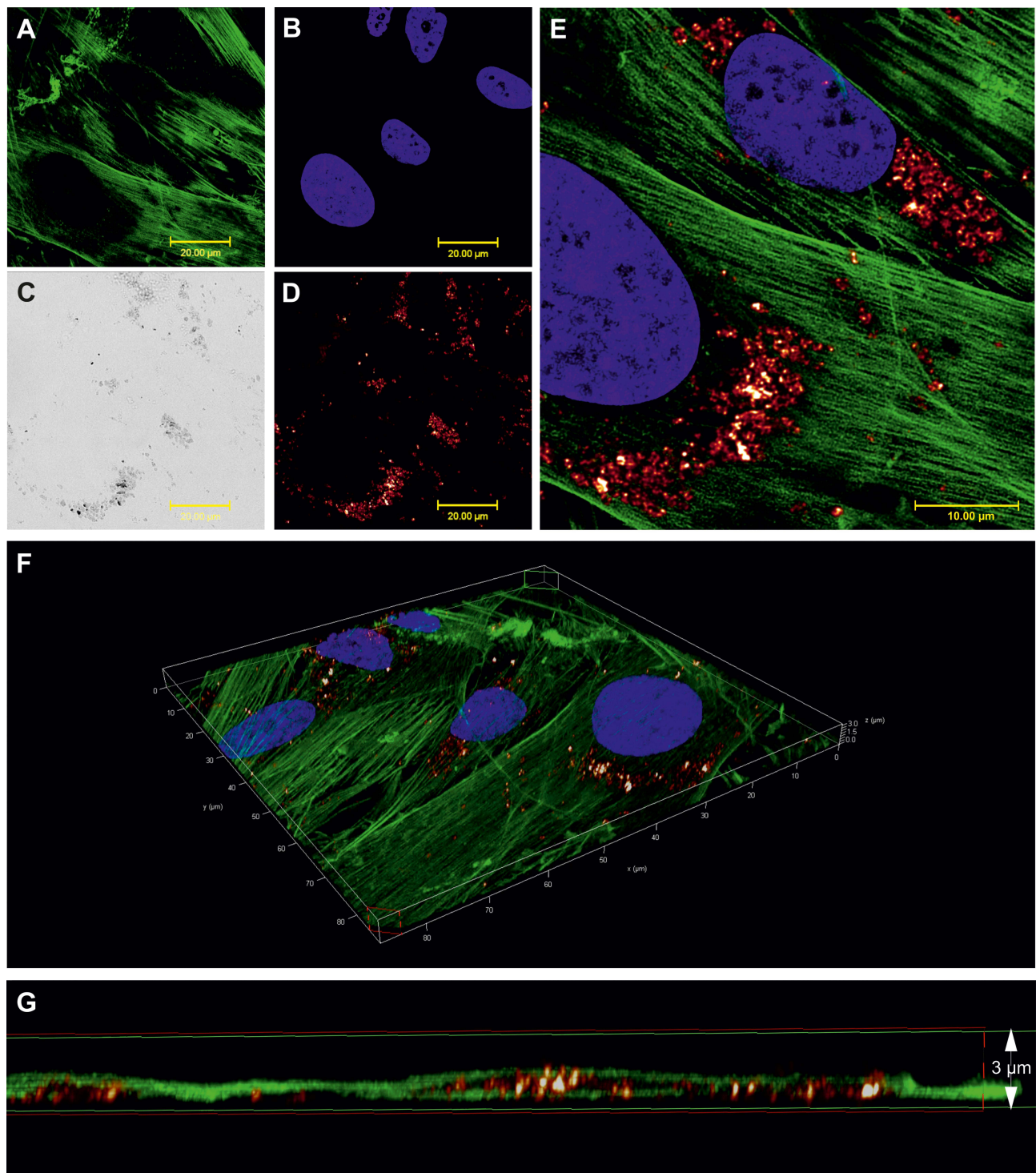


**Figure 2** Cellular uptake of nanoparticles (SPION<sup>PAM</sup>). (A–E) Imaging of SPION-labeled cells using (A and B) fluorescence labelling (A: phalloidin, green; B: Hoechst, blue), (C) transmission (grey) and (D) reflectance (glow) mode. (E) Merged and detailed view of the sample showed in (A–D). (F and G) Image sections of the 3D video ([Supplementary Video 1](#)) from the sample shown in (A–E). For materials and methods see supplement. Images were captured by Karl-Heinz Körtje at Leica Microsystems GmbH.

precancerous cells, CRM potentially enables screening, detection, and therapy of serious diseases. Similarly, Kah et al synthesized AuNPs coupled with anti-EGFR as molecular contrast probes for imaging biomolecular changes during carcinogenesis.<sup>55</sup> In the in vitro experiments, they compared the localization of gold bioconjugates in nasopharyngeal carcinoma CNE2 cells and normal human lung fibroblasts and showed that CNE2 cells, in contrast to normal fibroblasts,

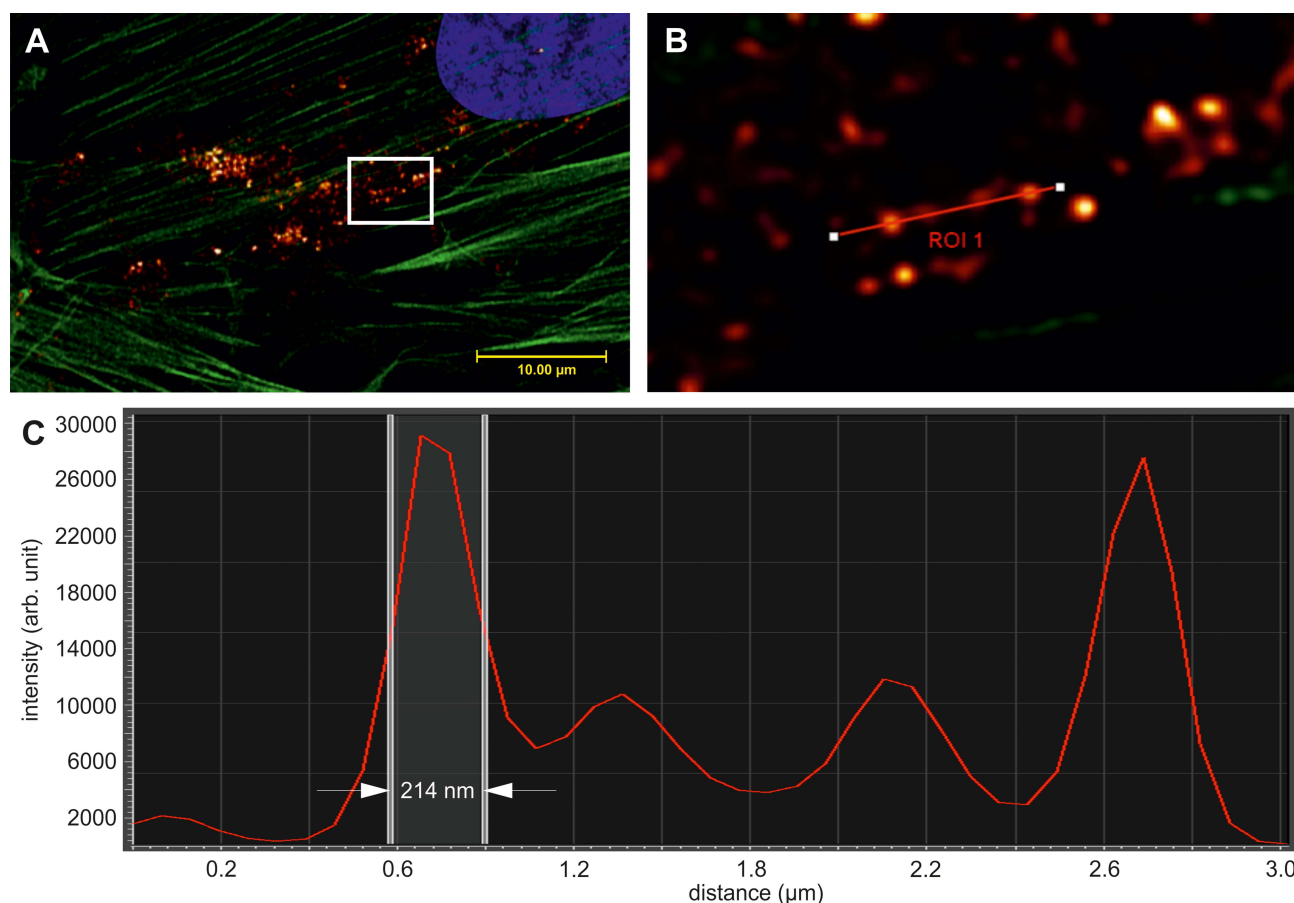


**Figure 3** Image resolution of SPION<sup>PAM</sup> clusters. **(A and B)** SPION<sup>PAM</sup>-labelled cells. **(B)** Magnified reflectance image of the framed section in **(A)**. **(C)** Intensity profile in the region of interest (ROI 1) in **(B)** indicating the full width half maximum of the selected nanoparticle objects. For materials and methods see supplement. Images were captured by Karl-Heinz Körtje at Leica Microsystems GmbH.

**Abbreviations:** arb. unit, arbitrary unit; ROI, region of interest.

had domains of increased reflectance corresponding to increased cellular EGFR expression. Finally, Cid-Barrio et al used CRM for ultrasensitive quantification of disease biomarkers in complex biological samples.<sup>56</sup> To this end, they developed a sandwich immunoassay platform for the detection of prostate specific antigen (PSA), a cancer biomarker. PSA was bound by capture antibodies and its detection was realized by antibodies coupled to Mn-ZnS quantum dots (QDs) or gold nanoparticles. To achieve high sensitivity, controlled catalytic gold deposition was subsequently performed on the surface of the NPs. The resulting surface magnification enabled an amplification of the reflected light, dramatically lowering the detection limit of the PSA.

### Quantitative Confocal Reflectance Microscopy (Q-CRM)

The quantification of the particles contained in cells or tissues is crucial in biomedical research. Conventional methods to determine the amount of unlabeled metal-based NPs mostly rely on spectroscopic techniques, such as atomic emission or absorption spectroscopy (AES or AAS). Those methods are very accurate, but have the disadvantage that they can only analyze the total amount of metal atoms in the sample. Lack of information about the extracellular or intracellular localization of the NPs constitutes a serious disadvantage. Among other methods, TEM is very expensive, has a very small field of view, and requires extensive sample preparation. CRM can be used as an alternative method to investigate and quantify the uptake of NPs, as shown in a study by Mazzolini et al. The uptake of nanoceria (CeO<sub>2</sub>-NPs), which is present in combustion engine exhaust and potentially affects cells of the respiratory tract, was investigated in different lung-derived cells.<sup>57</sup> Results of that study indicated that the presence of a protein corona promotes internalization of nanoceria by clathrin-mediated endocytosis and prevents cytotoxicity. In contrast, in serum-free media and the absence of

a protein corona, nanoceria cause disruption of the plasma membrane and alterations in cell metabolism. As already mentioned above, AuNPs are increasingly used as nanomarkers in biological systems. The study by Klein et al aimed to define parameters that enable visualization and quantification of colloidal and intracellular AuNPs using a conventional confocal laser scanning microscopy (CLSM) and surface plasmon resonance (SPR)-enhanced light scattering.<sup>58</sup> After the preparation of AuNPs and subsequent size separation by successive centrifugation steps, they showed that AuNPs with a size of 60 nm and larger were reliably detected by confocal microscopy. For particles of this size, the scattering cross-section of SPR can be visualized in individual particles and used to quantify the gold mass, through the size-dependent relationships between AuNP mass and particle numbers. AuNPs in size of 60 to 80 nm could also be quantified in different cell compartments, with a high probability of the separation of individual particles. In addition, gold causes a spectral shift to longer wavelengths in cells, and additional luminescence that can be used for NP visualization. Based on these phenomena, Kim et al presented a simple and rapid method using CLSM to provide real-time tracking of AuNPs and quantify the uptake of particles into cells.<sup>59</sup> The quantification, based on a linear relationship between scattering intensity and particle size, was confirmed by inductively coupled plasma mass spectrometry (ICP-MS).

## Dark-Field Microscopy (DFM)

Dark-field microscopy (DFM) selectively captures the light scattered from the sample while excluding the incident light.<sup>60</sup> As a result, the field around the sample produces a dark background while the sample is visualized as a bright object.<sup>40</sup> Numerous instrument configurations have been developed to excite nanoparticles in the far and near field based on this principle.<sup>60</sup> In a confocal microscope, the light illuminating the sample is focused through the objective and collected by a dark-field condenser. Based on the light scattering properties, even structures smaller than the diffraction limit deflect light and can therefore be detected with DFM. Accordingly, DFM is well suited for visualizing reflective NP, especially in combination with the capabilities of CLSM to resolve objects in the z-plane.<sup>40</sup>

Yoshimura et al demonstrated that DFM can be used for antibody detection and thus for the analysis of biomolecules and disease diagnosis.<sup>61</sup> Using bovine serum albumin (BSA) as a biological example, they showed that the detection of aggregation of BSA-functionalized AuNPs was already possible at an anti-BSA antibody concentration of 20 nM. After incubation of retinal pigment epithelial cells with AgNPs by DFM, Zucker et al observed the presence of cell-sized extracellular rings of deposited nanoparticles that frequently emerged near what appeared to be post mitotic daughter cells. The rings were most likely the result of NP binding to adhesion membrane proteins released during mitotic cytokinesis contraction that remained on the slide (Figure 4).<sup>62</sup> Thus, DFM could also serve as a tool for studying normal and abnormal mitosis.

Zhang and Monteiro-Riviere directly compared DFM and CLSM in reflection mode. In DFM, AgNP in the focal plane were imaged as bright spherical objects and AgNP outside the focal plane were relatively gray. On the other hand, in CLSM reflection mode, in-focus AgNP were very bright and AgNP outside the focus were non-visible.<sup>40</sup> Gibbs-Flournoy et al evaluated the potential of dark-field-CLSM to circumvent the drawbacks of fluorescence and electron microscopy in the assessment of toxic effects of non-fluorescent nanoparticles.<sup>63</sup> They demonstrated the spatial colocalization of fluorescence (confocal) and scattered transmitted light (dark-field) along all axes and showed the feasibility of visualizing cellular TiO<sub>2</sub> nanoparticle uptake and localization, relative to intracellular organelles, in cultured human lung cells.

DFM can also be used to detect exposure to various metal oxide NPs. Guttenberg et al used enhanced DFM (EDFM) with improved alignment and focus of oblique angle illumination to analyze the biodistribution of inhaled engineered amorphous silica (SiO<sub>2</sub>), alumina (Al<sub>2</sub>O<sub>3</sub>), or ceria (CeO<sub>2</sub>) NPs in a rat model of occupational exposure.<sup>64</sup> Amin et al developed a multifocal microscopy (MFM) system composed of a dark-field/bright-field illumination, a laser illumination, and multifocal scanning that allows rapid three-dimensional imaging of biological specimen and nanoparticles by simultaneously acquiring micrographs from multiple focal planes.<sup>65</sup> The use of a spatial light modulator (SLM) as a multifocal grating and a special SLM calibration algorithm enabled very high intensity uniformity, which provides an alternative to the use of conventionally fabricated gratings in MFM. However, DF-CLSM also has its limitations. For example, accurate size determination of NPs and their number in agglomerates is limited because other factors, such as surface irregularities and reflectivity, considerably affect the signal strength in dark-field detection.



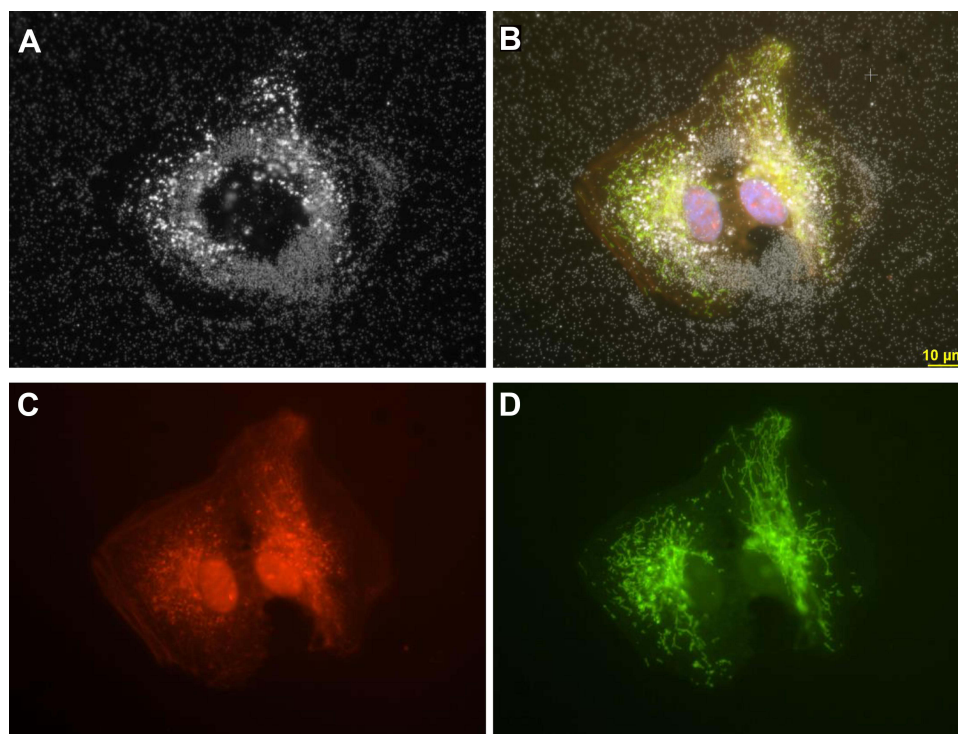


**Figure 4** Retinal pigment epithelial cells (ARPE-19) incubated with 3 µg/mL AgNP. (A) Darkfield image, (B) Merged image of (C and D) and DAPI staining, (C) CellMask Orange plasma membrane staining, (D) Cells transfected with Mito-GFP (green). Magnification 600x. Pictures were done by darkfield optics using a 60-x plan Fluor objective with an iris diaphragm (NA 0.55–0.90). Reproduced from Zucker RM, Ortenzio J, Degn LL, Boyes VK. Detection of large extracellular silver nanoparticle rings observed during mitosis using darkfield microscopy. *PLoS One*. 2020;15(12):e0240268. The work is made available under the Creative Commons CC0 public domain dedication<sup>62</sup>.

## Differential Interference Contrast Microscopy (DICM)

Phase-sensitive microscopy allows visualization of weakly scattered samples with low contrast and is widely used in biological and medical research. Differential interference contrast microscopy (DICM) is frequently utilized to study the interactions between cells and NPs, particularly their cellular uptake.<sup>66,67</sup> The DIC mode of confocal microscopes can also be used to detect individual NPs. However, in contrast to DFM, DICM usually produces images with very low contrast compared to the background.<sup>40</sup> Meanwhile, DICM has been further developed and refined, and even allows quantitative phase contrast imaging of bio-samples, detection of nanoparticles, and determination of the RI of microbeads.<sup>68</sup>

DICM can also be utilized to monitor biosensors, particularly gold nanorods and more complex-structured AuNPs. It also allows deciphering the rotational motions at the cellular and molecular levels resulting from wavelength- and angle-dependent optical patterns of NPs in DIC images.<sup>69–72</sup> For instance, Choo et al described a three-step finite-difference time-domain simulation method for DICM of anisotropic metal NPs that can be extended to predict DIC images of NPs with different morphologies, composition, and dielectric environment. Such approach is promising for studying the motion of single particles in solutions or cellular environments.<sup>69</sup> Another study established a computational imaging platform to determine the 3D orientation of anisotropic optical nanoprobe based on acquired DICM images.<sup>73</sup> The model predicted the orientation of nanorods with a high degree of accuracy and has the potential to enable a robust, rapid, and fully automated tracking of particle rotations during interaction with living cells.

Culver et al investigated the structural characteristics of gold nanostars using DICM and proved that the DIC image patterns allow the discrimination between symmetric and asymmetric 2D and 3D structures of individual nanostars and can thus be exploited to observe the orientation of NPs.<sup>74</sup> A single-particle correlation study using DFM and DICM to characterize the optical properties of gold nanostars was performed by Kim et al.<sup>75</sup> They demonstrated that single gold nanostars can be used either as individual sensors with DIC polarization anisotropy, or as multispectral orientation probes



to obtain detailed information on rotational motions and rotational speeds at their localized SPR wavelengths in fast dynamic studies. Bhowmik et al used DICM to investigate the translational and rotational dynamics of functionalized gold nanostars interacting with cells in serum-containing medium.<sup>76</sup> They found that gold nanostars with targeted ligands exhibited a greater dynamic effect and higher rotational speed on cell membranes compared to gold nanostars with non-targeted ligands. The study also revealed that despite similar protein adsorption profiles, the targeted interactions are preserved in the presence of a protein corona.

Beyond imaging, DICM allows reliable analysis of blood-based biomarkers. As an example, Roy et al established a microarray platform for highly sensitive and selective detection of disease-specific circulating miRNAs in human serum, without the need for RNA extraction, labeling, and target amplification.<sup>77</sup> The dedicated target-specific hairpin capture probes enabled a reliable discrimination of miRNA sequences, and a DICM-supported nanoparticle-based detection method enabled a resolution down to a single molecule.

## Optical Coherence Tomography (OCT)

Three-dimensional reflection microscopy has long been introduced into the clinics. Decades ago, Huang et al presented a non-invasive, non-destructive, reflectance technique called optical coherence tomography (OCT), which uses low-coherence interferometry to generate tomographic images of optical scattering from tissue microstructures, such as retinal structures and coronary arteries with atherosclerotic plaques.<sup>78</sup> Specifically, in low-coherence reflectometry, the coherence property of light which is reflected at the boundaries of differing RIs of a sample delivers information on the time-of-flight delay from the reflecting boundaries and backscattering sites. The time delay information is then utilized to specify the longitudinal location of the reflective sites with high accuracy and resolution. After running multiple longitudinal scans at a series of lateral locations, the OCT system creates a two-dimensional map of the sample's reflective sites. The optical sectioning capability of OCT is comparable to that of CRM. However, OCT is limited only by the coherence length of the light source and enables high-depth resolution and thus non-invasive in vivo deep tissue imaging and sectioning of biological tissues. In addition, a combination of OCT and CRM provides even higher accuracy in imaging deeper structures, for example, to distinguish between normal skin morphology and tumor-related pathologies, which has greatly improved the prevention and detection of skin diseases and epithelial carcinomas.<sup>79</sup> Accordingly, this technique could be useful for imaging NP distribution in tissues.

In order to improve the accuracy of differentiation between normal and neoplastic tissue in skin cancer diagnosis, AuNPs are frequently used for contrast enhancement in OCT images. During the topical administration, the contrast agent should be distributed and absorbed into the skin as efficiently as possible. Xu et al demonstrated that the combination of DMSO and sonophoresis is a very effective method to improve the diffusion and penetration rate of AuNPs in porcine skin ex vivo.<sup>80</sup> Coughlin et al developed gadolinium-conjugated gold-silica nanoshells to improve both the diagnosis and image-guided photothermal therapy of cancer.<sup>81</sup> The particles allowed multimodal imaging by X-ray, MRI, CRM, two-photon luminescence, as well as OCT. Tucker-Schwartz et al also presented a multimodal imaging platform using photothermal OCT to perform high-resolution in vivo imaging of intravenously injected gold nanorods and detected their accumulation in mouse mammary tumors.<sup>82</sup> Nguyen et al used arginine-glycine-aspartic acid peptide (RGD)-conjugated AuNP clusters as a biocompatible, intravenous contrast agent for multimodal OCT and photoacoustic microscopy (PAM). Using the developed particles, newly formed blood vessels in the retina of rabbits were visualized with low background and high contrast and resolution.<sup>83</sup>

In addition to gold-based contrast agents, other metals are also used in OCT imaging. Marin et al produced a dark OCT contrast agent based on plasmonic copper sulfide NPs that have virtually no light scattering at approximately 1300 nm and absorb only the examination light, resulting in dark contrast.<sup>84</sup> The results demonstrated the potential of dark contrast OCT for light-controlled biomedical applications. Kumar et al used TiO<sub>2</sub> NPs as a contrast agent with nonspecific binding combined with a high-speed OCT system at 1060 nm for in vitro imaging of animal tissue.<sup>85</sup> This system, allowing good tissue penetration enabling observation of deeper layers and a very good contrast-to-noise ratio, could thus serve to distinguish different tissue types and their alterations. As another example application, polymeric microneedles provide an option for transdermal drug delivery, but their real-time microscopic monitoring is difficult. Therefore, Seeni et al incorporated Fe<sub>3</sub>O<sub>4</sub> NPs as a contrast agent into polymeric polystyrene-*block*-poly (acrylic acid)

microneedles, improving the contrast-to-noise ratio in OCT imaging by a factor of 10.<sup>86</sup> Cimalla et al developed a combined setup of magnetomotive OCT (MM-OCT), laser speckle reflectometry, and light microscopy for in vivo monitoring of therapeutically administered Fe<sub>3</sub>O<sub>4</sub> NP-labeled mesenchymal stem cells, which are potential candidates for stem cell therapy in regenerative medicine.<sup>87</sup>

In addition to the commonly used application of OCT to study skin and skin diseases, the technique can also be used to examine vascular systems by using flexible imaging probes such as catheters and endoscopes. For example, Hu et al utilized gold nanoshells as contrast agents for intravascular OCT imaging and demonstrated its capability for three dimensional visualization and real time tracking of individual nanoshells within a 0.9 mm diameter catheter under both dynamic and static conditions.<sup>88</sup>

## Photothermal Microscopy (PTM)

Photothermal microscopy (PTM) exploits the slight changes in RI due to the absorption of a light beam and enables a highly sensitive detection of individual non-fluorescent particles and molecules.<sup>29,89–92</sup> Photothermal detection of small absorbing markers is free of background noise even in scattering environments, and could enable true single-molecule measurements over very long time periods.<sup>93</sup> Furthermore, by combining the enantioselective signal of circular dichroism with the high sensitivity of PTM, the technique is even capable of identifying chiral nano-objects.<sup>94</sup> In PTM, the contribution of the scattered field from NPs is usually not considered. Shi et al demonstrated that both the heat-induced intensity variation of the scattered light from Ag nanowires and the intensity increase of the reflected light caused by the thermal lens contribute to the PT signal obtained.<sup>95</sup> Li et al developed a resonant scattering-enhanced PTM approach in which the imaged nano-objects were nearly resonant with the probe laser light.<sup>96</sup> This allowed resonant scattering enhanced PT imaging of plasmonic NPs with ultra-high sensitivity.

Boyer et al showed that far-field optical detection of gold colloids down to 2.5 nm is possible using a photothermal method that combines high-frequency modulation and polarization interference contrast.<sup>93</sup> Thus, a photothermal microscope is capable of detecting particles down to a few nanometers.

The use of photothermal lens microscopy in combination with a microchip enabled a successful application of a highly sensitive DNA detection method based on AuNPs.<sup>97</sup> The method can be further developed for the detection of single-base-pair mismatches between a probe and a target, which is very important for the detection of single nucleotide polymorphisms.

Another photothermal technique is AFM-IR, which combines atomic force microscopy (AFM) and infrared (IR) spectroscopy.<sup>98</sup> This method allows the determination of the spatial resolution of tens of nanometers as well as the analysis of the chemical composition of a sample. In the tapping AFM-IR mode, it is possible to obtain information not only on the morphology and composition of the NP, but also on the location of the incorporated active ingredients and the core-shell structures. The method is therefore suitable as a potential tool for quality control of NP formulations.

The detection of biological nanoparticles, such as vesicular stomatitis viruses (VSV) and poxviruses, was realized by Zhang et al using a confocal interferometric mid-infrared photothermal imaging system.<sup>99</sup> For this purpose, the very weak photothermal signal resulting from the infrared absorption of chemical bonds was detected using the interferometric scattering principle. The differences in the fingerprint IR spectra even allowed label-free spectroscopic differentiation of biological particles. However, the imaging speed of PTM is usually not high enough to image processes in living cells. Gao et al used the so-called absorption-modulated scattering microscopy (AMSM), which exploits both the resonance absorption and scattering properties of plasmonic NPs.<sup>100</sup> AMSM had the ability to effectively remove the light scattering background, such as the cellular component, and significantly increased the imaging speed compared to conventional laser scanning PTM, which enabled real-time imaging of NPs below 10 nm in living cells at 20 fps.

Monitoring of cancer therapy and its effects on cells is crucial for evaluating the therapeutic progress. Wang et al developed a PT sensor based on DNA-templated AuNP-QD complexes for imaging and labeling of cancer cells.<sup>101</sup> Since the photoluminescence signal of the QDs is retained in the cells even after treatment, it provides durable photothermal labeling for cell tracking and enables image-based therapy evaluation. Based on nonlinear signal dependence on the laser energy, Nedosekin et al presented a super-resolution far-field PTM that allowed resolutions down to 50 nm and was able to resolve multiple nanostructures including plasmonic nanoparticles and hemoglobin nanoclusters in red blood cells.<sup>102</sup>

Bijeesh et al developed a confocal microscope based on a photothermal effect induced by two-photon absorption that is capable of detecting cellular barium titanate ( $\text{BaTiO}_3$ )-NPs with high sensitivity and could potentially be used for imaging in deep tissue.<sup>103</sup> In addition to fluorescence and photoacoustic microscopy (PAM), PTM was also used as part of a multimodal imaging approach to investigate the penetration of gold nanorods into multicellular 3D tissue spheroids derived from human pancreatic stromal cells.<sup>104</sup> The results revealed that the cells serve as a physical and/or chemical barrier and accordingly only allow a very low penetration of the particles into the spheroid. Chang et al synthesized neodymium vanadate/gold heterojunction nanocrystals with very good Vis/NIR absorption and high cytotoxicity under NIR laser irradiation, which could act as a potential anticancer agent.<sup>105</sup> Due to the ability to convert light to heat and the thermal expansion effect, the nanocrystals also offer superior dual PT/PA imaging ability.

## Holographic Microscopy (HGM)

Holographic microscopy (HGM) is a laser technique which generates a 3D RI holotomogram and allows the precise localization of objects such as microorganisms, cells, and NPs, as well as measurement of surface profiles, RIs and even quantification of the size of individual particles.<sup>106–109</sup> The hologram is a result of the interference of coherent light scattered from an object with a mutually coherent reference beam. The image is obtained either by “in-line” imaging, in which the object and reference beams are aligned, or by “off-axis” imaging, in which the two beams interfere at an angle.<sup>110</sup> Subsequent 3D reconstruction of the original object field allows accurate localization of the NPs in the sample.<sup>111</sup>

Flewellen et al presented a digital transmission holographic microscope that can switch between inline mode (eg, to track motile bacteria), off-axis dark-field holography (eg, to localize NPs), and bright-field off-axis mode (eg, to measure the RI and dry mass of objects via quantitative phase recovery).<sup>106</sup> Liebel et al presented a holographic Raman scattering microscope based on the coupling of an interferometer with a holographic microscope.<sup>112</sup> The microscope simultaneously recorded the phase and amplitude of the wide-field images of multiple surface-enhanced Raman scattering (SERS) NPs along with their respective Raman spectra, allowing localization and tracking of individual NPs in living cells. By using a recently developed holographic transient microscope, which allows a reliable discrimination between non-resonant dielectric and resonant metallic nanoparticles, the same group demonstrated an ultrafast identification, visualization and tracking of unlabeled nanoparticles in the presence of nonspecific scattering, which is thus potentially applicable to living cells and tissues.<sup>113,114</sup>

Kalies et al developed a multimodal imaging and manipulation setup combining fluorescent and holographic imaging, allowing a correlative morphological and physiological analysis during laser irradiation of AuNP-labeled cells.<sup>115</sup> Monitoring of the cellular impact with digital holography revealed a shrinkage of cell volume and area, possibly due to cytoplasmic outflow. The method could be useful for the development and implementation of applications such as AuNP-mediated laser transfection, or photothermal therapy. For potential cancer cell therapy, Narayanaswamy and Torchilin developed immunoliposomes functionalized with a monoclonal cancer-specific antibody (mAb) 2C5 and loaded with the chemotherapeutic agents paclitaxel and salinomycin.<sup>116</sup> Cellular morphology, proliferation, and cell division of breast cancer cells after treatment with the modified liposomes were monitored by holographic imaging over 48 h and demonstrated therapeutic efficacy of the liposomal formulation.

Commonly, only the added particle amount is reported in studies of NP cytotoxicity, which is either referring to the medium volume (mg/mL) or the cell culture area ( $\text{mg}/\text{cm}^2$ ).<sup>15</sup> However, depending on the colloidal stability of the particles, a significantly different particle concentration may prevail at the plasma membrane. Additionally, the actual intracellular particle dose differs from the concentration in the medium, although it has been shown that this can correlate.<sup>15</sup> Direct measurement of the amount of incorporated particles would therefore be very useful for evaluating their biocompatibility. G  lo  n showed that unlabeled nanodiamonds can be detected and localized in cells by measuring the RI.<sup>117</sup> In a former study from our group, Friedrich et al used holotomographic images to determine the intracellular content of unlabeled NPs in various SPION-labeled pancreatic cancer cells, by quantifying the areas of high RI.<sup>33</sup> The results closely corresponded to quantitative iron measurement by AES, demonstrating the reliability of the method. Moreover, in contrast to AES and quantitation via flow-cytometric side scatter analysis, it allowed the discrimination between membrane-bound and intracellular particles. In a further study, the same approach was used to quantify the uptake of various SPIONs in different head and neck squamous cell carcinoma cell lines in response to an external magnetic field.<sup>66</sup>

## Photoacoustic Microscopy (PAM)

Photoacoustic microscopy (PAM) combines the high spatial and temporal resolution of ultrasound with the good contrast and multiplexing capabilities of optical imaging.<sup>118</sup> In PAM, incident light and the absorption of photons causes thermal expansion and hence a pressure difference causing a photoacoustic effect. The contrast can be significantly increased by endogenous and exogenous contrast agents, such as hemoglobin, melanin, methylene blue, Prussian blue, phthalocyanine, naphthalocyanine, or various NPs.<sup>118–120</sup> In contrast to the often very low optical absorption and photoacoustic signal of small molecules, inorganic or organic/polymeric NPs have usually a strong and stable signal and are frequently used, for example, as probes to track biological processes or to label proteins and other substances.<sup>29,118,119</sup>

Ma et al developed ratiometric semiconducting polymer NPs (RSPNPs) which exhibited enhanced photoacoustic signals at about 690 nm after reaction with  $O_2^{\bullet-}$ , whereas the signal at 800 nm served as an internal photoacoustic reference.<sup>121</sup> Experiments with apolipoprotein E-deficient mice indicated that RSPNPs could be used to evaluate the rupture risk of atherosclerotic plaques caused by acute pneumonia by determining the oxidative stress level within aortic atherosclerosis. Wang et al developed herceptin-conjugated Poly (lactide-co-glycolic acid)-Polyethylene glycol (PLGA-PEG) NPs loaded with  $SiO_2$ -coated gold nanorods and perfluorohexane liquid as therapeutic agent for laser-induced vaporization treatment and therapy of HER2-positive breast cancer.<sup>122</sup> In vitro and in vivo experiments using PAM demonstrated the efficient targeting of the particles to HER2-positive cells and mouse tumors. Also aiming at breast cancer therapy, Fu et al prepared doxorubicin (DOX)-loaded mesoporous Prussian blue NPs doped with the nitric oxide-producing prodrug sodium nitroprusside (NO-PB).<sup>123</sup> The authors showed that the release of encapsulated DOX was pH-dependent and that the particles produced NO molecules in cells, accumulated in tumor tissue, and could be imaged by PAM.

For NP-based photothermal therapy and photoacoustic imaging, St Lorenz et al developed nanoparticle systems containing various near-infrared (NIR) heptamethine cyanine dyes, which were incorporated into polymeric NPs to provide water solubility and protection of their photophysical characteristics.<sup>124</sup> In another study, iron-copper doped polyaniline NPs were synthesized, in which the Cu (II) undergoes a redox reaction with glutathione, highly elevated in tumor tissues.<sup>125</sup> This results in a red shift of the absorption spectrum of the NPs enabling a simultaneous photoacoustic tumor imaging and photothermal therapy. Beside those examples mentioned above, many other studies also recently utilized NPs as theranostic nanoplatforms, enabling photothermal therapy and photoacoustic imaging.<sup>126,127</sup>

The advantage of PAM is its compatibility with many other imaging modalities, which allows combination of real-time monitoring in cells and nanoparticle-based therapies. For instance, colloidal RGD-conjugated AuNPs served as contrast agents for PAM and OCT to visualize newly formed blood vessels in the retina of rabbits.<sup>83</sup> For tumor vessel imaging, Xu et al used the intrinsic properties of hemoglobin for PA imaging and ultrasound imaging to gain information about blood flow.<sup>128</sup> A dual contrast agent based on alginate-hydrogel microdroplets encapsulating conjugated polymeric NPs enabled a detailed blood flow mapping in tumor microvessels of mice with clear tumor edges. Miao et al developed a multimodal infrared fluorescent and photoacoustic contrast agent based on a fluorescent NP copolymer with a high photothermal conversion efficiency for photothermal therapy.<sup>129</sup> As theranostics against hepatocellular carcinoma, Li et al constructed a multifunctional molecular probe from iRGD-modified phase transformation lipid nanoparticles loaded with the chemotherapeutic agent 10-hydroxycamptothecin.<sup>130</sup> The NPs demonstrated their suitability for dual ultrasound/PA imaging and the ability of tumor targeting, deep penetration into the tumor, and drug release under focused low-intensity ultrasound.

## Total Internal Reflection Microscopy (TIRM)

Light incident at a flat angle from an optically dense medium into a less dense medium, eg a glass-water interface, generates an evanescent wave by total internal reflection (TIR).<sup>60</sup> TIRM exploits evanescent wave illumination to obtain high-contrast images of a thin optical section above a substrate (usually a cover slip).<sup>131,132</sup> Although the technique is similar to darkfield microscopy, TIRM can be used to obtain additional information about the size and depth of scattering sites on, or near, the surface.<sup>133</sup> In contrast to total internal reflection fluorescence microscopy (TIRFM), TIRM detects reflected light rather than fluorescence. However, both techniques can be combined to allow simultaneous live visualization of unlabeled nanoparticles and fluorescently-labeled plasma membrane structures. Byrne et al used TIRM/TIRFM to study clathrin-mediated endocytosis of polystyrene colloids.<sup>134</sup> They found that there is an upper limit of particle size for cellular uptake in 3T3 fibroblast cells, as particles of 500 nm in diameter were associated with clathrin before and during cellular internalization, whereas this was not



evident for larger colloids 1  $\mu\text{m}$  in diameter. Chakkarapani demonstrated a highly sensitive TIR-based nanoarray chip for the serum detection of cancer antigen 125 (CA125), which is an indicator of the stage of various cancers, including ovarian cancer.<sup>135</sup> Direct comparison between TIRM and TIRFM using AgNPs and AlexaFluor 488 labeling revealed clear advantages of plasmonic NP labeling, which showed much higher resistance to photobleaching, better photostability, and higher signal-to-noise ratio compared to fluorescent labeling.

Braslavsky et al used a dark-field illumination setup of an objective-type TIRM to achieve a total internal reflection DFM (TIRDFM) for detecting 20 nm gold particles and tracking the motion of 60-nm polystyrene beads.<sup>136</sup> Nan et al used a similar modification of a TIRM for two-dimensional tracking of gold NPs with microsecond temporal resolution and nanometer spatial precision to visualize kinesin and dynein motions.<sup>137</sup> Mickolajczyk and Hancock described the construction of a TIRDFM for high-speed, in vitro single-molecule kinesin tracking.<sup>138</sup> Ando et al achieved angstrom-level precision of AuNP localization and microsecond time resolution with TIRDFM of AuNPs. The system was successfully used to observe the motion of kinesin-1, and may thus also enable the analysis and further understanding of the dynamics of biomolecular motors. TIRDFM has also been used for single-molecule detection using micro- or nanoparticles and fluorescent markers as optical probes. In the study of Ueno et al, such a system was used to study the rotational mechanism of the molecular motor  $F_1$ -ATPase.<sup>139</sup> They were able to visualize the fluctuation of an AuNP bound to the  $\gamma$ -subunit of  $F_1$ -ATPase during catalytic dwell and the stepping motion during torque generation with microsecond temporal precision and nanometer spatial precision. Thus, TIRDFM could be used to study many biophysical processes that require high temporal and spatial resolution.

Ryu et al utilized TIRM to detect the absorption of target molecules to NPs.<sup>140</sup> The recognition was based on the shift of the localized SPR (LSPR) scattering spectrum after chemisorption of 1-alkanethiols with different chain lengths to single plasmonic gold nanorods (AuNRs) with the same diameter and different aspect ratios. They also demonstrated that the absorbed compounds were detected more sensitively at the inflection point, at the long-wavelength side of the LSPR scattering peak, than at the conventionally used peak maximum of the LSPR. In another study, a fast quantitative detection method for hypochlorite anions ( $\text{ClO}^-$ ) as a model substance was developed by combining the near-infrared luminescence energy transfer of upconversion nanoprobes with the upconversion luminescence TIR platform.<sup>141</sup> Since the excitation wavelength is not near the ultraviolet range, as is common with TIRFM, but in the near-infrared at 980 nm, excessive cytotoxicity is prevented.

Jiang et al presented a TIR-based leakage radiation microscopy using leakage radiation from evanescent TIR waves for rapid label-free in situ monitoring of nanopollutants in the environment.<sup>142</sup> This technique enabled imaging of individual polystyrene and Au nanospheres with diameters as small as 100 and 30 nm, respectively. Li et al reported a TIR-based extinction spectroscopy technique to determine the extinction spectra of individual dielectric, plasmonic, or light-absorbing nano-objects based on the interaction between a nanoparticle and an evanescent wave.<sup>143</sup> The advantages of the demonstrated technique include the simultaneous acquisition of the extinction spectra of multiple nanoparticles using only a low power density of the incident light. Finally, Andr  n et al used TIRM to study interactions between a glass surface and individual gold nanoparticles trapped with laser tweezers. They showed the particles can be optically confined at controllable distances between  $\sim 30$  and  $\sim 90$  nm from the surface depending on the radiation pressure of the trapping laser and the ionic shielding of the surrounding liquid.<sup>144</sup> Control of particle spacing might be important, for instance, for applications where a nanoparticle could act as a separation-dependent localized heat source or as an optical antenna for sensing and analysis of nanoscale objects.<sup>144,145</sup>

## Surface Plasmon Resonance Microscopy (SPRM)

Noble metal NPs, like all other metal-based particles, possess the ability to scatter light and thus can be imaged by DFM. However, due to the interaction between the nanoparticles' conductive free electrons and the electromagnetic field of incident light, noble metals such as Au, Ag, Cu, and Al possess additional unique optical properties that can be exploited for particle imaging. When light falls on a single NP, the free electrons of the metal are forced to oscillate  $180^\circ$  out of phase relative to the momentary electric field of the light. The nuclei of the particle lattice then pull the electrons to return to their equilibrium position. However, the electrons overshoot the equilibrium and continue to oscillate back and forth. When the frequency of the incident light matches the frequency of this oscillation, a resonance condition is achieved, resulting in resonant light absorption

and scattering, referred to as LSPR.<sup>60,146–149</sup> For example, in spherical AuNPs, the resonance occurred in the visible spectral region at ~520 nm, leading to a brilliant red color in solution.

Due to their overall good biocompatibility, the possibility of surface functionalization with biomolecules and their tunable optical properties, AuNPs are suitable components of optical biosensors useful for many optical imaging techniques.<sup>29,60,150,151</sup>

Shang et al developed multilayer Au@MnO<sub>x</sub>@SiO<sub>2</sub> NPs as a pH-sensitive plasmonic nanosensor to study the dynamic acidification as well as perturbations of phagosome maturation in phagocytic cells. Such investigations are of importance which would be beneficial for many biological and physiological studies, eg on host defense and efficiency to eliminate pathogens.<sup>152</sup> The MnO<sub>x</sub> shell and outer SiO<sub>2</sub> served as sensing and protective layers that decompose in an acidic environment, resulting in an increased spectral shift and color change of the gold core in DFM. The dynamics of the color change indicated that the phagosome undergoes two distinct stages of slow to rapid acidification during the phagosome maturation process. Ghotra et al presented a miniaturized biosensor platform for selective detection of microRNA based on the disassembly of tightly coupled plasmonic core-satellite nanoparticle assemblies.<sup>153</sup> In their approach, binding of the nucleic acid results in dehybridization of the DNA linkers coupled to the gold particles and leads to changes in light scattering properties, which can be detected and analyzed using DFM. Such chip-based sensors could thus provide an alternative platform for mapping and quantitative detection of biomolecules, eg ATP, in the cellular microenvironment.

The plasmonic resonance properties of NPs can also be used for enhanced analysis of biopsy samples. Wang et al demonstrated the use of gold-silver alloy NPs and gold nanorods with defined plasmonic resonance properties, such as scattering efficiency and spectral position of the resonance peak, as a reliable tool for identifying and differentiating different NP markers by conventional dark-field NP imaging.<sup>154</sup> Ge et al analyzed the dynamic interactions of NPs on the cytoplasmic membrane by visualizing the translational and rotational diffusion of single anisotropic plasmonic nanoparticles using a dark-field microscope equipped with a color camera.<sup>155</sup> The method could potentially be used for the analysis and clarification of complicated biological processes in living cells.

## Rayleigh Light Scattering Microscopy (RLSM)

Compared to the LSPR of spherical NPs, the conductive free electron oscillation along both the long and short axes of rod-shaped noble metal NPs results in a stronger resonance band in the near-infrared region and a weaker band in the visible region.<sup>147</sup> At the resonance wavelength, the Rayleigh light scattering of individual NPs is enhanced many times their geometric size, enabling imaging and spectroscopy of individual NPs.<sup>146</sup> Thus, the features of Rayleigh scattering of NPs, including peak wavelength and spectral bandwidth, depends on the structural properties, composition and local environment of the NPs.<sup>150</sup> Microscopes with white light illumination and dark-field optics allow the discrimination of light scattering from individual NPs with different size and/or shape due to different optical resonances. Light scattering and absorption also depend on the environment, which allows the use of single NPs as a nanosensors for ultrasensitive detection of various biological and chemical analytes.<sup>156</sup>

Using a dark-field microspectroscopy system, Truong et al analyzed the relationship of Rayleigh scattering properties of single Au nanospheres and Au nanorods with their size, shape and local dielectric environment.<sup>147</sup> They demonstrated that the structural properties of a single AuNP of specific size and shape determine the resonant Rayleigh light scattering characteristics (such as the position of the spectral peak, the scattering cross-section, and the RI sensitivity), which may be useful for the design and fabrication of ultrasensitive LSPR nanosensors. In a study by Song et al, single AuNPs served as nanoplasmonic sensors for rapid, sensitive, and specific monitoring of molecular interactions between nucleic acids and promoters.<sup>157</sup> Binding of macromolecules to the surface of an AuNP was quantitatively detected by the maximum wavelength shift of LSPR. In another study, Rayleigh light scattering spectroscopy was used for highly sensitive detection of small molecule-sized proteins, such as lysozymes.<sup>158</sup> This was accomplished by detecting the binding and interaction of a DNA aptamer adsorbed on the surface of immobilized AuNPs with its target molecule resulting in plasmonic resonance coupling of the AuNPs. Louit et al used a Rayleigh confocal scattering spectroscopic imaging system to monitor the changes in spectral properties, such as transitory as well as plasmon resonance band shifts, of individual AuNPs resulting from interactions with live mouse fibroblasts. The change in spectral properties of individual AuNPs was linked to the formation of lipid layers close to the particle

surface during endocytosis and exocytosis.<sup>159</sup> In addition to the studies mentioned above, there are numerous other examples where resonance Rayleigh scattering has been used for very sensitive detection of a wide variety of proteins, nucleic acids, insecticides, pesticides, fungicides, and metal ions.<sup>156</sup>

## Hyperspectral Light Microscopy (HLM)

Hyperspectral imaging is not an optical principle in a proper sense, but refers to a technique for acquiring spectral data. By combining it with optical microscopy techniques such as fluorescence, brightfield, or darkfield microscopy, additional valuable information can thus be obtained about the sample being examined. Hyperspectral imaging sensors can record the UV/Vis, or infrared spectra from different locations very close to each other. The data sets obtained by this kind of spectroscopic imaging are usually arranged as data cuboids, where the x and y dimensions cover a specific area of a sample (spatial information) and the z dimension covers a specific wavelength range.<sup>160</sup> The spectrum of each pixel subsequently enables reliable assignment and identification of the recorded objects. The workflow of data analysis and mapping is presented in Figure 5.<sup>161</sup>

As mentioned, microscopes based on spectral identification of objects have the ability to reliably detect and track NPs, even in biological samples.<sup>16,60,162</sup> It is thus feasible to use these techniques in order to investigate the potential biological effects and health consequences of NP exposure, which are increasingly found in industrial processes and commercial products. Similarly, hyperspectral imaging can be used to detect nanoparticle contamination in plants wastewaters.<sup>163,164</sup> By using NP probes, hyperspectral light microscopy (HLM)-based systems are moreover suitable for diagnosis of diseases and therapy monitoring.

Patskovsky et al presented a hyperspectral imaging system for wide-field, dark-field and spectral examination of plasmonic NPs.<sup>165</sup> It was based on the principle of reflected light microscopy with illumination provided by a supercontinuum white light laser and a tunable filter for spectral filtering and scanning in the range from 400–1000 nm. The system was used for 3D localization of AuNPs functionalized with monoclonal antibodies against human CD44. The efficiency of the developed set-up was confirmed in cell preparations of CD44-expressing MDA-MB-231 human breast cancer cells.<sup>165</sup>

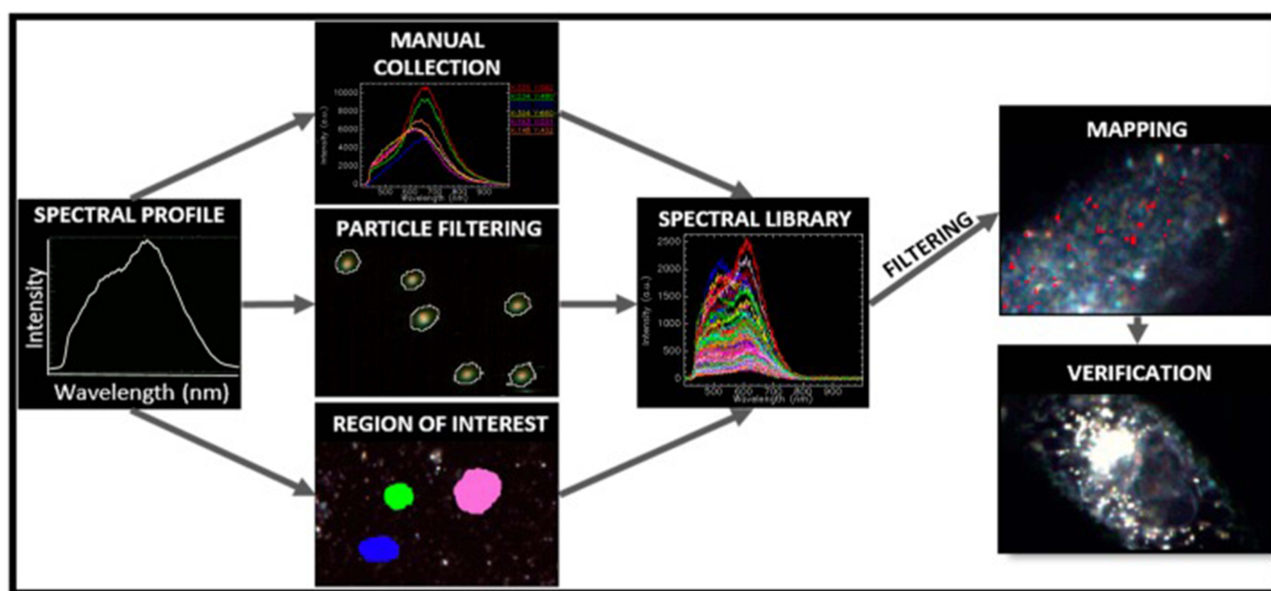


**Figure 5** Workflow of data analysis and mapping in hyperspectral microscopy.

**Notes:** Reproduced from Zamora-Perez P, Tsoutsis D, Xu R, Rivera\_Gil P. Hyperspectral-Enhanced Dark Field Microscopy for Single and Collective Nanoparticle Characterization in Biological Environments. *Materials*. 2018;11(2):243. Copyright © 2018 by the authors. Licensee MDPI, Basel, Switzerland. This article is an open access article distributed under the terms and conditions of the Creative Commons Attribution (CC BY) license (<http://creativecommons.org/licenses/by/4.0/>)<sup>161</sup>.

The hyperspectral technique is not only suitable for the detection of noble metal-based NPs with their unique reflectance spectra, but is also applicable to other metal or metal oxide nanoparticles, such as those made of alumina, silica, ceria, iron and silver, among others.<sup>162,166</sup> Beside metal-based nanoparticles, hyperspectral light microscopy (HLM) can be utilized for the detection of particles made of polymers and peptides.<sup>167,168</sup> Once reference spectra of known materials are obtained and collected into spectral libraries, the samples can be analyzed using HLM and matched with the reference spectra to determine the location and composition of the NPs.

Peña Mdel et al used hyperspectral microscopy to capture the spectrum from 400 to 1000 nm at each pixel in an enhanced DFM image (EDFM-HSI).<sup>169</sup> The method was used to localize, identify, and map metal oxide nanomaterials *ex vivo* in porcine skin tissues, a toxicological model for cutaneous exposure to metal oxide nanomaterials. The EDFM-HSI results were confirmed by other methods, including Raman spectroscopy (RS), scanning electron microscopy (SEM), and energy-dispersive X-ray spectroscopy (EDS). Idelchik et al used HLM data based on enhanced DFM to verify different HLM classification algorithms for industrial ceria nanoparticles (CeO<sub>2</sub>NPs) in lung tissue of rats exposed to NP inhalation.<sup>170</sup> The study showed that sample preparation and sample matrices significantly affected the thresholds for classification of NP. Therefore, algorithms should be carefully selected based on specific material and matrix properties to achieve reliable classification results. Touloumes et al increased the imaging contrast for mapping unlabeled TiO<sub>2</sub> and ZnO nanoparticles in human skin sections by tissue clearing with organic solvents, which reduced background light scattering caused by the extracellular matrix.<sup>171</sup> The distribution of the NPs was imaged by dark-field, bright-field, and confocal microscopy and on a dark-field hyperspectral microscope integrated with a confocal Raman microscope in transmission mode. A study by Zucker et al utilized hyperspectral imaging, among other techniques, to investigate cellular uptake, intercellular agglomeration, and morphological effects of differently coated AgNPs.<sup>172</sup> Their data demonstrated that hyperspectral DFM was capable of detecting changes in the composition of the protein corona after cellular internalization of NPs. In line with this, Persaud et al showed that the spectrum of internalized AgNPs exhibited a red shift and peak broadening compared to non-internalized ones, indicating the association of cellular macromolecules.<sup>173</sup>

The use of extended dark-field hyperspectral imaging (EDF-HSI) can even be used to detect nanomaterials from biomolecules whose optical scattering properties are only slightly different from the structures in their vicinity. For example, Liu et al demonstrated that the optical scattering intensity of peptide-based nanoparticles can be significantly increased by prior amidation of the peptides, and thus can be easily visualized and tracked by EDF-HSI even in cells and nematodes.<sup>167</sup>

In nanomedical research, more and more particles are produced as carriers of bioactive substances or as contrast agents, which have to be investigated in appropriate assays to evaluate their impact on cells. In the study by Hosseinidoust et al, after synthesis and characterization of different cellulose nanocrystals, cellular uptake of unlabeled particles was detected by dark-field hyperspectral microscopy and fluoresceinamine-conjugated NPs using confocal microscopy.<sup>174</sup> An important requirement in the medical application of NPs is their blood stability, since the particles are usually administered intravenously. The study of particle aggregation in blood can be well evaluated microscopically. A rapid method for measuring aggregation behavior of plasmonic AuNPs in blood was presented by Jenkins et al.<sup>175</sup> They used results from DFM with hyperspectral detection, confocal Raman microscopy (CRM), and single particle inductively-coupled plasma mass spectrometry (spICP-MS) to distinguish primary particles from agglomerates. The preparation of spectral maps showed that the scattering peak of primary AuNPs appeared at ~550–560 nm, small agglomerates at ~580 nm, and large agglomerates at ~550 nm and ~660–700 nm.

Nano- and microparticles can also pose a serious ecological threat that can severely affect the health of living organisms. These include the increasing pollution of water by nano- and microplastics, which has been increasing for decades. In their study, Nigamatzyanova and Fakhrullin demonstrated the identification of synthetic polymer particles by dark-field hyperspectral microscopy. With this technique, polystyrene, polymethacrylate, and melamine formaldehyde particles could be effectively imaged and identified in water samples. Also, *in vivo* reliable visualization and spectral identification of chemically distinct types of nano- and microplastics in a *Caenorhabditis elegans* nematode model of particle uptake and tissue distribution was demonstrated, providing another method to detect nano- and microplastics in the environment and their biological distribution and toxicological effects in tissues and organs.<sup>168</sup>



The application of artificial intelligence is increasingly finding its way into data analysis. Ishmukhametov et al used the application of deep learning algorithms for the classification of polystyrene microparticles differing only in pigmentation using a residual neural network and enhanced DFM. After training the neural network model, the accuracy of the obtained classification algorithm was up to 93% in cell samples from human skin fibroblasts treated with microplastics. The technique could thus be an alternative to current spectral-based methods for identifying microplastic particles in living cells and organisms, which are usually very time-consuming.<sup>176</sup>

## Reflectance Structured Illumination Microscopy (R-SIM)

A super-resolution microscopy technique called structured illumination microscopy (SIM) uses grid projections to increase the diffraction-induced resolution limit by a factor of two or more and enables the identification of previously unresolvable cellular structures such as single nuclear pore complexes or microtubules.<sup>177–179</sup> Accordingly, by using reflection techniques, SIM can also provide the resolution for imaging NP-cell interactions.

Chang et al adopted 3D-SIM for scattered light imaging of gold NPs in HeLa cells and achieved improved image quality at a resolution below the diffraction limit.<sup>180</sup> A commercial SIM microscope was used by Guggenheim et al to accomplish super-resolution reflectance imaging with an X-Y resolution of 115 nm, thereby resolving closely spaced NP clusters (Figure 6).<sup>181</sup> They also demonstrated that combining dynamic live reflectance and fluorescence imaging data (obtained with CRM, R-SIM) with TEM images can provide additional information about NP-cell interactions and thus be useful for imaging and understanding processes such as endocytosis, vesicle transport, ligand/receptor interactions, and disease pathogenesis. In another study, Guggenheim et al demonstrated that administered SPIONs are efficiently

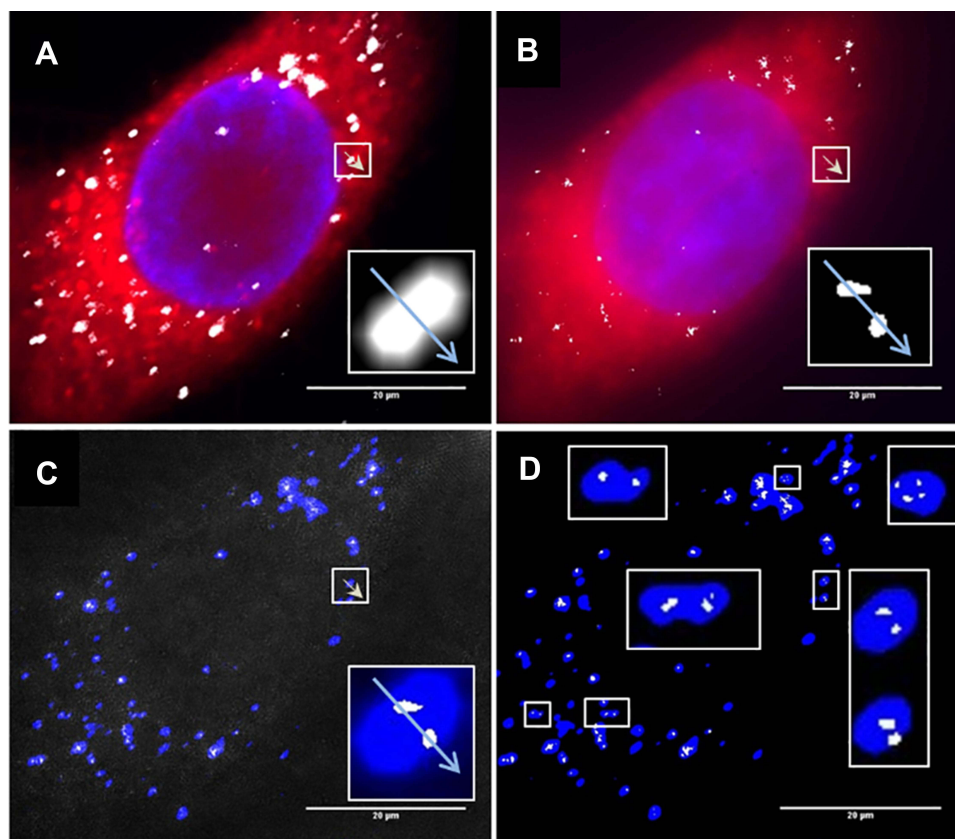


**Figure 6** Sensitivity of Confocal Reflectance Microscopy (CRM) and Reflectance Structured Illumination Microscopy (R-SIM). HeLa cells were treated with cerium dioxide NPs. (A) CRM and (B) R-SIM show cytoplasmic stain (CTDR, red), nuclear stain (DAPI, blue) and NP signal (grey). Overlay of the cerium dioxide NP regions show particles detected in CRM (blue) and SIM (grey) in both the raw (C) and processed (D) images. White boxes display a sample of regions where CRM detects one spot and SIM detects multiple spots, illustrating the enhanced resolution of SIM. Reproduced from Guggenheim EJ, Khan A, Pike J, Chang L, Lynch I, Rappoport JZ. Comparison of Confocal and Super-Resolution Reflectance Imaging of Metal Oxide Nanoparticles. PLoS One. 2016;11(10):e0159980. © 2016 Guggenheim et al. This is an open access article distributed under the terms of the Creative Commons Attribution License<sup>181</sup>.

internalized into several cell lines, regardless of whether they are macrophages or cancer cells.<sup>182</sup> Using CRM and R-SIM, they revealed that SPION uptake in cancer cells involves both caveolar-mediated endocytosis and macropinocytosis, whereas in macrophages the clathrin-dependent pathway is more predominant. Accordingly, detailed knowledge of the uptake, localization, transport, and fate of NPs could significantly improve their therapeutic or diagnostic potential and reduce off-target effects.

## Quantum Microscopy: An Exciting Perspective for Imaging at the Low Nm Range

The quantum sensing (QS) technique provides an opportunity to have the intrinsic properties of SPIONs available for high resolution imaging in the atomic resolution range. The most commonly applied quantum system for quantum sensing is the nitrogen vacancy center (NV-center) in diamond.<sup>183–188</sup> It belongs to the class of color defects, which is formed by substitutional nitrogen atom adjacent to carbon vacancy in the diamond lattice, with  $C_{3v}$  symmetry around one of the four {111} crystallographic directions. The preferred internal energetic structure and photophysics of the NV-center enables optical initialization, readout and coherent manipulation with long spin coherence time at ambient conditions. From a quantum mechanical point of view, the Stark shift and electron Zeemann shift are the most important physical effects. Based on these effects, the NV-center can be used as a very sensitive quantum sensor. So far, applications of NV-centers are mainly found in materials science and process engineering where they serve, for example, as ultrasensitive pressure- or temperature sensors, or are used as electrometers. The application takes advantage of the specific features of QS, which are (i) high magnetic sensitivity, (ii) operation at ambient conditions, (iii) high resolution, and (iv) calibration free operation.<sup>188–193</sup> Those are the reasons why several attempts have been recently made to adapt this technology for other fields of application, especially in biomedical research, including imaging at the cellular level. *Per se*, quantum microscopy is not a technology that works as native imaging, but it is indispensably dependent on the imaging substrate, which in this case consists of magnetizable particles. The metrological advantages as described above can only be realized if SPIONs can be precisely positioned with a minimum of non-specific accumulation. A key work in this context was done by Barbiero et al who succeeded in highlighting fixed cells nonspecifically using SPIONs, which were ligated with nanodiamonds, and thus making them visible via a NV-center based widefield microscope.<sup>194</sup> In this approach, SPIONs carried out a part of the detector, but were not able to selectively mark the cells. Specific labelling of living cells and tracing them in real-time in living tissues via their magnetic signature is a challenge that has not been tackled so far. To achieve this, significant efforts in SPIONs material development, NV-detector adaptation and suitability testing on a wide variety of cellular and tissue targets need to be addressed. If the selective binding of SPIONs is achieved, those particles can be harnessed for cellular imaging, unprecedented insights into physiological mechanisms may be possible, with implications for a wide range of biomedical research areas.

## Conclusions

Since the effects of nanomaterials strongly depend on their physicochemical properties, which are dictated in particular by the surface chemistry, there has been a growing concern about the appropriateness of using labeled NPs to evaluate the biological behavior and impact of their label-free counterparts. Further factor aggravating this issue is that unbound labels may be present in the nanoparticle solution and that even adherent labels can dissociate, ultimately leading to incorrect evaluation of particle localization and quantification.<sup>9,195,196</sup>

This is particularly important for biocompatibility studies of NPs intended for medical applications, because ultimately, unless the fluorescence property is explicitly relevant to the application, the unlabeled particles will be administered. This implies that the entire workflow, starting with in vitro toxicological experiments and cellular particle uptake, to in vivo biodistribution, tolerance and efficacy studies should ideally be performed with unlabeled particles to enable successful translation to the clinic. Accordingly, methods for reliable visualization of unlabeled NPs are of growing importance.

In the last decades, there have been many innovative developments in label-free visualization of nanomaterials. Meanwhile, virtually all major microscopy manufacturers also offer configurations with which this is possible. Apart from this, there are many proprietary developments by working groups that are used for specific research purposes. There have also been several reports of multimodal systems in which two or more imaging techniques have been combined.

Hence, a wide range of possibilities for determining and visualizing the effects of NPs, as well as for evaluating their safety is now increasingly available.

However, most detection systems do not provide an absolute proof that a certain signal really originates from a nanoparticle, since the methods are based on light reflection or scattering. This means that other structures with a high RI, such as dust or even distinct components of cells and tissues, can produce a similar signal. Therefore, in addition to mandatory control samples, it is important to ensure that all solutions and materials used, especially cell culture media, wash solutions, slides and coverslips, have as little impurities as possible. The advantage of these techniques lies in the fact that the very dependence on the RI allows simultaneous label-free imaging of different cellular constituents together with NPs and may, therefore, provide complementary information on the organization and structure of biological samples.

With the ongoing efforts, it is likely that the existing systems will be continuously improved and new techniques will be developed to study unlabeled NPs within their biological environment faster, with greater reliability, and at even higher resolution.

## Acknowledgments

The authors thank Barbara Leibbrandt and Karl-Heinz Körtje at Leica Microsystems GmbH for microscopic imaging and support. We are also very grateful to Julia Band and Eveline Schreiber from SEON at the Universitätsklinikum Erlangen for help with cell culture and nanoparticle production. We thank the Else Kröner Fresenius Stiftung, Bad Homburg v.d. H., Germany (2018\_A88) for their support. We acknowledge Deutsche Forschungsgemeinschaft and Friedrich-Alexander-Universität Erlangen-Nürnberg for their support within the funding programme “Open Access Publication Funding”.

## Author Contributions

All authors made a significant contribution to the work reported, whether that is in the conception, study design, execution, acquisition of data, analysis and interpretation, or in all these areas; took part in drafting, revising or critically reviewing the article; gave final approval of the version to be published; have agreed on the journal to which the article has been submitted; and agree to be accountable for all aspects of the work.

## Disclosure

The authors report no conflicts of interest in this work.

## References

1. Elahi N, Rizwan M. Progress and prospects of magnetic iron oxide nanoparticles in biomedical applications: a review. *Artif Organs*. 2021;45(11):1272–1299. doi:10.1111/aor.14027
2. Tietze R, Zaloga J, Unterweger H, et al. Magnetic nanoparticle-based drug delivery for cancer therapy. *Biochem Biophys Res Commun*. 2015;468(3):463–470. doi:10.1016/j.bbrc.2015.08.022
3. Jose J, Kumar R, Harilal S, et al. Magnetic nanoparticles for hyperthermia in cancer treatment: an emerging tool. *Environ Sci Pollut Res Int*. 2020;27(16):19214–19225. doi:10.1007/s11356-019-07231-2
4. Cores J, Caranasos TG, Cheng K. Magnetically targeted stem cell delivery for regenerative medicine. *J Funct Biomater*. 2015;6(3):526–546. doi:10.3390/jfb6030526
5. Abdal Dayem A, Lee SB, Cho SG. The impact of metallic nanoparticles on stem cell proliferation and differentiation. *Nanomaterials*. 2018;8(10):10. doi:10.3390/nano8100761
6. Kumari S, Sharma N, Sahi SV. Advances in cancer therapeutics: conventional thermal therapy to nanotechnology-based photothermal therapy. *Pharmaceutics*. 2021;13(8):1174. doi:10.3390/pharmaceutics13081174
7. Mitchell MJ, Billingsley MM, Haley RM, Wechsler ME, Peppas NA, Langer R. Engineering precision nanoparticles for drug delivery. *Nat Rev Drug Discov*. 2021;20(2):101–124. doi:10.1038/s41573-020-0090-8
8. Chen F, Ehlerding EB, Cai W. Theranostic nanoparticles. *J Nucl Med*. 2014;55(12):1919–1922. doi:10.2967/jnumed.114.146019
9. Nam J, Won N, Bang J, et al. Surface engineering of inorganic nanoparticles for imaging and therapy. *Adv Drug Deliv Rev*. 2013;65(5):622–648. doi:10.1016/j.addr.2012.08.015
10. Abarca-Cabrera L, Fraga-Garcia P, Berensmeier S. Bio-nano interactions: binding proteins, polysaccharides, lipids and nucleic acids onto magnetic nanoparticles. *Biomater Res*. 2021;25(1):12. doi:10.1186/s40824-021-00212-y
11. Natarajan P, Tomich JM. Understanding the influence of experimental factors on bio-interactions of nanoparticles: towards improving correlation between in vitro and in vivo studies. *Arch Biochem Biophys*. 2020;694:108592. doi:10.1016/j.abb.2020.108592
12. Wolfram J, Zhu M, Yang Y, et al. Safety of nanoparticles in medicine. *Curr Drug Targets*. 2015;16(14):1671–1681. doi:10.2174/1389450115666140804124808

13. Padmanabhan P, Kumar A, Kumar S, Chaudhary RK, Gulyas B. Nanoparticles in practice for molecular-imaging applications: an overview. *Acta Biomater.* 2016;41:1–16. doi:10.1016/j.actbio.2016.06.003
14. Heidt T, Nahrendorf M. Multimodal iron oxide nanoparticles for hybrid biomedical imaging. *NMR Biomed.* 2013;26(7):756–765. doi:10.1002/nbm.2872
15. Friedrich RP, Janko C, Poettler M, et al. Flow cytometry for intracellular SPION quantification: specificity and sensitivity in comparison with spectroscopic methods. *Int J Nanomedicine.* 2015;10:4185–4201. doi:10.2147/IJN.S82714
16. Gajdosechova Z, Mester Z. Recent trends in analysis of nanoparticles in biological matrices. *Anal Bioanal Chem.* 2019;411(19):4277–4292. doi:10.1007/s00216-019-01620-9
17. Rad AM, Janic B, Iskander AS, Soltanian-Zadeh H, Arbab AS. Measurement of quantity of iron in magnetically labeled cells: comparison among different UV/VIS spectrometric methods. *BioTechniques.* 2007;43(5):627–628, 630, 632 passim. doi:10.2144/000112599
18. Wiekhorst F, Steinhoff U, Eberbeck D, Trahms L. Magnetorelaxometry assisting biomedical applications of magnetic nanoparticles. *Pharm Res.* 2012;29(5):1189–1202. doi:10.1007/s11095-011-0630-3
19. Dadashzadeh ER, Hobson M, Henry Bryant L Jr, Dean DD, Frank JA. Rapid spectrophotometric technique for quantifying iron in cells labeled with superparamagnetic iron oxide nanoparticles: potential translation to the clinic. *Contrast Media Mol Imaging.* 2013;8(1):50–56. doi:10.1002/cmmi.1493
20. Poller JM, Zaloga J, Schreiber E, et al. Selection of potential iron oxide nanoparticles for breast cancer treatment based on in vitro cytotoxicity and cellular uptake. *Int J Nanomedicine.* 2017;12:3207–3220. doi:10.2147/IJN.S132369
21. Mayhew TM, Muhlfeld C, Vanhecke D, Ochs M. A review of recent methods for efficiently quantifying immunogold and other nanoparticles using TEM sections through cells, tissues and organs. *Ann Anat.* 2009;191(2):153–170. doi:10.1016/j.aanat.2008.11.001
22. Stender AS, Marchuk K, Liu C, et al. Single cell optical imaging and spectroscopy. *Chem Rev.* 2013;113(4):2469–2527. doi:10.1021/cr300336e
23. Gunn J, Paranjli RK, Zhang M. A simple and highly sensitive method for magnetic nanoparticle quantitation using <sup>1</sup>H-NMR spectroscopy. *Biophys J.* 2009;97(9):2640–2647. doi:10.1016/j.bpj.2009.08.013
24. Kurokawa K, Nakano A. Live-cell Imaging by Super-resolution Confocal Live Imaging Microscopy (SCLIM): simultaneous three-color and four-dimensional live cell imaging with high space and time resolution. *Bio Protoc.* 2020;10(17):e3732. doi:10.21769/BioProtoc.3732
25. Feng H, Wang X, Xu Z, Zhang X, Gao Y. Super-resolution fluorescence microscopy for single cell imaging. *Adv Exp Med Biol.* 2018;1068:59–71.
26. Igarashi M, Nozumi M, Wu LG, et al. New observations in neuroscience using superresolution microscopy. *J Neurosci.* 2018;38(44):9459–9467. doi:10.1523/JNEUROSCI.1678-18.2018
27. Yin L, Wang W, Wang S, Zhang F, Zhang S, Tao N. How does fluorescent labeling affect the binding kinetics of proteins with intact cells? *Biosens Bioelectron.* 2015;66:412–416. doi:10.1016/j.bios.2014.11.036
28. Ostrowski A, Nordmeyer D, Boreham A, et al. Overview about the localization of nanoparticles in tissue and cellular context by different imaging techniques. *Bellstein J Nanotechnol.* 2015;6:263–280. doi:10.3762/bjnano.6.25
29. Wu Y, Ali MRK, Chen K, Fang N, El-Sayed MA. Gold nanoparticles in biological optical imaging. *Nano Today.* 2019;24:120–140. doi:10.1016/j.nantod.2018.12.006
30. Wang W. Imaging the chemical activity of single nanoparticles with optical microscopy. *Chem Soc Rev.* 2018;47(7):2485–2508. doi:10.1039/C7CS00451F
31. Fakhrullin R, Nigamatzyanova L, Fakhrullina G. Dark-field/hyperspectral microscopy for detecting nanoscale particles in environmental nanotoxicology research. *Sci Total Environ.* 2021;772:145478. doi:10.1016/j.scitotenv.2021.145478
32. Mehta N, Sahu SP, Shaik S, Devireddy R, Gartia MR. Dark-field hyperspectral imaging for label free detection of nano-bio-materials. *Wiley Interdiscip Rev Nanomed Nanobiotechnol.* 2021;13(1):e1661. doi:10.1002/wnan.1661
33. Friedrich RP, Schreiber E, Tietze R, Yang H, Pilarsky C, Alexiou C. Intracellular quantification and localization of label-free iron oxide nanoparticles by holotomographic microscopy. *Nanotechnol Sci Appl.* 2020;13:119–130. doi:10.2147/NSA.S282204
34. Gaspar I, Szabad J. In vivo analysis of MT-based vesicle transport by confocal reflection microscopy. *Cell Motil Cytoskeleton.* 2009;66(2):68–79. doi:10.1002/cm.20334
35. Pimenta R, Soares-de-almeida L, Arzberger E, et al. Reflectance confocal microscopy for the diagnosis of skin infections and infestations. *Dermatol Online J.* 2020;26(3):1.
36. Calzavara-Pinton P, Longo C, Venturini M, Sala R, Pellacani G. Reflectance confocal microscopy for in vivo skin imaging. *Photochem Photobiol.* 2008;84(6):1421–1430. doi:10.1111/j.1751-1097.2008.00443.x
37. White WM, Baldassano M, Rajadhyaksha M, et al. Confocal reflectance imaging of head and neck surgical specimens. A comparison with histologic analysis. *Arch Otolaryngol Head Neck Surg.* 2004;130(8):923–928. doi:10.1001/archotol.130.8.923
38. Guggenheim EJ, Lynch I, Rappoport JZ. Imaging in focus: reflected light imaging: techniques and applications. *Int J Biochem Cell Biol.* 2017;83:65–70. doi:10.1016/j.biocel.2016.12.008
39. Dunn AK, Smithpeter C, Welch AJ, Richards-Kortum R. Sources of contrast in confocal reflectance imaging. *Appl Opt.* 1996;35(19):3441–3446. doi:10.1364/AO.35.003441
40. Zhang LW, Monteiro-Riviere NA. Use of confocal microscopy for nanoparticle drug delivery through skin. *J Biomed Opt.* 2013;18(6):061214. doi:10.1117/1.JBO.18.6.061214
41. Rajadhyaksha M, Grossman M, Esterowitz D, Webb RH, Anderson RR. In vivo confocal scanning laser microscopy of human skin: melanin provides strong contrast. *J Invest Dermatol.* 1995;104(6):946–952. doi:10.1111/1523-1747.ep12606215
42. Rajadhyaksha M, Gonzalez S, Zavislan JM, Anderson RR, Webb RH. In vivo confocal scanning laser microscopy of human skin II: advances in instrumentation and comparison with histology. *J Invest Dermatol.* 1999;113(3):293–303. doi:10.1046/j.1523-1747.1999.00690.x
43. Maitland KC, Gillenwater AM, Williams MD, El-Naggar AK, Descour MR, Richards-Kortum RR. In vivo imaging of oral neoplasia using a miniaturized fiber optic confocal reflectance microscope. *Oral Oncol.* 2008;44(11):1059–1066. doi:10.1016/j.oraloncology.2008.02.002
44. Ando Y, Sakurai T, Koida K, et al. In vivo bioluminescence and reflectance imaging of multiple organs in bioluminescence reporter mice by bundled-fiber-coupled microscopy. *Biomed Opt Express.* 2016;7(3):963–978. doi:10.1364/BOE.7.000963
45. Fuchs CSK, Ardigo M, Haedersdal M, Mogensen M. In vivo reflectance confocal microscopy of gold microparticles deposited in the skin. A case report on cutaneous chrysiasis. *Lasers Surg Med.* 2020;52(1):13–16. doi:10.1002/lsm.23179



46. Stensberg MC, Madangopal R, Yale G, et al. Silver nanoparticle-specific mitotoxicity in *Daphnia magna*. *Nanotoxicology*. 2014;8(8):833–842. doi:10.3109/17435390.2013.832430
47. Xu L, Wang YY, Huang J, Chen CY, Wang ZX, Xie H. Silver nanoparticles: synthesis, medical applications and biosafety. *Theranostics*. 2020;10(20):8996–9031. doi:10.7150/thno.45413
48. Tardillo Suárez V, Karepina E, Chevallet M, et al. Nuclear translocation of silver ions and hepatocyte nuclear receptor impairment upon exposure to silver nanoparticles. *Environ Sci*. 2020;7(5):1373–1387.
49. Wagner T, Kroll A, Haramagatti CR, Lipinski HG, Wiemann M. Classification and segmentation of nanoparticle diffusion trajectories in cellular micro environments. *PLoS One*. 2017;12(1):e0170165. doi:10.1371/journal.pone.0170165
50. Wagner T, Kroll A, Wiemann M, Lipinski HG. Classification of nanoparticle diffusion processes in vital cells by a multifeature random forests approach: application to simulated data, darkfield, and confocal laser scanning microscopy. Paper presented at: Proceedings of SPIE - The International Society for Optical Engineering; 2016.
51. Blumler P, Friedrich RP, Pereira J, Baun O, Alexiou C, Mailander V. Contactless nanoparticle-based guiding of cells by controllable magnetic fields. *Nanotechnol Sci Appl*. 2021;14:91–100. doi:10.2147/NSA.S298003
52. Friedrich RP, Zaloga J, Schreiber E, et al. Tissue plasminogen activator binding to superparamagnetic iron oxide nanoparticle-covalent versus adsorptive approach. *Nanoscale Res Lett*. 2016;11(1):297. doi:10.1186/s11671-016-1521-7
53. Friedrich RP, Janko C, Unterweger H, Lye S, Alexiou C. SPIONs and magnetic hybrid materials: synthesis, toxicology and biomedical applications. *Phys Sci Rev*. 2021. doi:10.1515/psr-2019-0093
54. Sokolov K, Follen M, Aaron J, et al. Real-time vital optical imaging of precancer using anti-epidermal growth factor receptor antibodies conjugated to gold nanoparticles. *Cancer Res*. 2003;63(9):1999–2004.
55. Kah JC, Olivo MC, Lee CG, Sheppard CJ. Molecular contrast of EGFR expression using gold nanoparticles as a reflectance-based imaging probe. *Mol Cell Probes*. 2008;22(1):14–23. doi:10.1016/j.mcp.2007.06.010
56. Cid-Barrio L, Ruiz Encinar J, Costa-Fernandez JM. Catalytic gold deposition for ultrasensitive optical immunosensing of prostate specific antigen. *Sensors*. 2020;20(18):18. doi:10.3390/s20185287
57. Mazzolini J, Weber RJ, Chen HS, et al. Protein corona modulates uptake and toxicity of nanoceria via clathrin-mediated endocytosis. *Biol Bull*. 2016;231(1):40–60. doi:10.1086/689590
58. Klein S, Petersen S, Taylor U, Rath D, Barcikowski S. Quantitative visualization of colloidal and intracellular gold nanoparticles by confocal microscopy. *J Biomed Opt*. 2010;15(3):036015. doi:10.1117/1.3461170
59. Kim CS, Li X, Jiang Y, et al. Cellular imaging of endosome entrapped small gold nanoparticles. *MethodsX*. 2015;2:306–315. doi:10.1016/j.mex.2015.06.001
60. Al-Zubeidi A, McCarthy LA, Rafiei-Miandashti A, Heiderscheid TS, Link S. Single-particle scattering spectroscopy: fundamentals and applications. *Nanophotonics*. 2021;10(6):1621–1655. doi:10.1515/nanoph-2020-0639
61. Yoshimura K, Maeda M, Kamiya N, Zako T. Protein-functionalized gold nanoparticles for antibody detection using the darkfield microscopic observation of nanoparticle aggregation. *Anal Sci*. 2021;37(3):507–511. doi:10.2116/analsci.20SC12
62. Zucker RM, Ortenzio J, Degn LL, Boyes WK. Detection of large extracellular silver nanoparticle rings observed during mitosis using darkfield microscopy. *PLoS One*. 2020;15(12):e0240268. doi:10.1371/journal.pone.0240268
63. Gibbs-Flournoy EA, Bromberg PA, Hofer TP, Samet JM, Zucker RM. Darkfield-confocal microscopy detection of nanoscale particle internalization by human lung cells. *Part Fibre Toxicol*. 2011;8(1):2. doi:10.1186/1743-8977-8-2
64. Guttenberg M, Bezerra L, Neu-Baker NM, et al. Biodistribution of inhaled metal oxide nanoparticles mimicking occupational exposure: a preliminary investigation using enhanced darkfield microscopy. *J Biophotonics*. 2016;9(10):987–993. doi:10.1002/jbio.201600125
65. Amin MJ, Petry S, Yang H, Shaevitz JW. Uniform intensity in multifocal microscopy using a spatial light modulator. *PLoS One*. 2020;15(3):e0230217–e0230217. doi:10.1371/journal.pone.0230217
66. Balk M, Haus T, Band J, et al. Cellular SPION Uptake and Toxicity in Various Head and Neck Cancer Cell Lines. *Nanomaterials*. 2021;11(3):726. doi:10.3390/nano11030726
67. Devereux SJ, Chung S, Daly HC, O'Shea DF, Quinn SJ. Multimodal microscopy distinguishes extracellular aggregation and cellular uptake of single-walled carbon nanohorns. *Chemistry*. 2018;24(53):14162–14170. doi:10.1002/chem.201801532
68. Ding C, Li C, Deng F, Simpson G. *Polarization Wavefront Shaping for Quantitative Phase Contrast Imaging by axially-Offset Differential Interference Contrast (ADIC) Microscopy*. Vol. 10887. SPIE; 2019.
69. Choo P, Hryn AJ, Culver KS, Bhowmik D, Hu J, Odom TW. Wavelength-dependent differential interference contrast inversion of anisotropic gold nanoparticles. *J Phys Chem C Nanomater Interfaces*. 2018;122(47):27024–27031. doi:10.1021/acs.jpcc.8b08995
70. Kim GW, Ha JW. Polarization-sensitive single dipoles generated from multiple sharp branches on the surfaces of single gold nanorods. *J Phys Chem C*. 2017;121(36):19975–19982. doi:10.1021/acs.jpcc.7b06823
71. Lee SY, Han Y, Hong JW, Ha JW. Single gold bipyramids with sharp tips as sensitive single particle orientation sensors in biological studies. *Nanoscale*. 2017;9(33):12060–12067. doi:10.1039/C7NR03969G
72. Zhao F, Chen K, Dong B, Yang K, Gu Y, Fang N. Localization accuracy of gold nanoparticles in single particle orientation and rotational tracking. *Opt Express*. 2017;25(9):9860–9871. doi:10.1364/OE.25.009860
73. Hu J, Liu T, Choo P, et al. Single-nanoparticle orientation sensing by deep learning. *ACS Cent Sci*. 2020;6(12):2339–2346. doi:10.1021/acscentsci.0c01252
74. Culver KSB, Liu T, Hryn AJ, Fang N, Odom TW. In situ identification of nanoparticle structural information using optical microscopy. *J Phys Chem Lett*. 2018;9(11):2886–2892. doi:10.1021/acs.jpclett.8b01191
75. Kim GW, Ha JW. Single gold nanostars with multiple branches as multispectral orientation probes in single-particle rotational tracking. *Chem Commun*. 2021;57(26):3263–3266. doi:10.1039/D1CC00731A
76. Bhowmik D, Culver KSB, Liu T, Odom TW. Resolving single-nanoconstruct dynamics during targeting and nontargeting live-cell membrane interactions. *ACS Nano*. 2019;13(12):13637–13644. doi:10.1021/acsnano.9b03144
77. Roy S, Soh JH, Ying JY. A microarray platform for detecting disease-specific circulating miRNA in human serum. *Biosens Bioelectron*. 2016;75:238–246. doi:10.1016/j.bios.2015.08.039
78. Huang D, Swanson EA, Lin CP, et al. Optical coherence tomography. *Science*. 1991;254(5035):1178–1181. doi:10.1126/science.1957169

79. Iftimia N, Peterson G, Chang EW, Maguluri G, Fox W, Rajadhyaksha M. Combined reflectance confocal microscopy-optical coherence tomography for delineation of basal cell carcinoma margins: an ex vivo study. *J Biomed Opt.* 2016;21(1):16006. doi:10.1117/1.JBO.21.1.016006
80. Xu Q, Jalilian E, Fakhoury JW, et al. Monitoring the topical delivery of ultrasmall gold nanoparticles using optical coherence tomography. *Skin Res Technol.* 2020;26(2):263–268. doi:10.1111/srt.12789
81. Coughlin AJ, Ananta JS, Deng N, Larina IV, Decuzzi P, West JL. Gadolinium-conjugated gold nanoshells for multimodal diagnostic imaging and photothermal cancer therapy. *Small.* 2014;10(3):556–565. doi:10.1002/smll.201302217
82. Tucker-Schwartz JM, Beavers KR, Sit WW, Shah AT, Duvall CL, Skala MC. In vivo imaging of nanoparticle delivery and tumor microvasculature with multimodal optical coherence tomography. *Biomed Opt Express.* 2014;5(6):1731–1743. doi:10.1364/BOE.5.001731
83. Nguyen VP, Qian W, Li Y, et al. Chain-like gold nanoparticle clusters for multimodal photoacoustic microscopy and optical coherence tomography enhanced molecular imaging. *Nat Commun.* 2021;12(1):34. doi:10.1038/s41467-020-20276-z
84. Marin R, Lifante J, Vazquez Besteiro L, et al. Plasmonic copper sulfide nanoparticles enable dark contrast in optical coherence tomography. *Adv Healthcare Mater.* 2020;9(5):1901627. doi:10.1002/adhm.201901627
85. Kumar A, Mondal I, Roy P, Poddar R. TiO<sub>2</sub> nanoparticles as exogenous contrast agent for 1  $\mu$ m swept source optical coherence tomography: an in vitro study. *Laser Phys.* 2018;28:035601. doi:10.1088/1555-6611/aa9cc9
86. Seeni RZ, Yu X, Chang H, Chen P, Liu L, Xu C. Iron oxide nanoparticle-powered micro-optical coherence tomography for in situ imaging the penetration and swelling of polymeric microneedles in the skin. *ACS Appl Mater Interfaces.* 2017;9(24):20340–20347. doi:10.1021/acsami.7b00481
87. Cimalla P, Werner T, Winkler K, et al. Imaging of nanoparticle-labeled stem cells using magnetomotive optical coherence tomography, laser speckle reflectometry, and light microscopy. *J Biomed Opt.* 2015;20(3):036018. doi:10.1117/1.JBO.20.3.036018
88. Hu J, Rivero F, Torres RA, et al. Dynamic single gold nanoparticle visualization by clinical intracoronary optical coherence tomography. *J Biophotonics.* 2017;10(5):674–682. doi:10.1002/jbio.201600062
89. Adhikari S, Spaeth P, Kar A, Baaske MD, Khatua S, Orrit M. Photothermal microscopy: imaging the optical absorption of single nanoparticles and single molecules. *ACS Nano.* 2020;14(12):16414–16445. doi:10.1021/acsnano.0c07638
90. Vermeulen P, Cognet L, Lounis B. Photothermal microscopy: optical detection of small absorbers in scattering environments. *J Microsc.* 2014;254(3):115–121. doi:10.1111/jmi.12130
91. Chien MH, Brameshuber M, Rossboth BK, Schutz GJ, Schmid S. Single-molecule optical absorption imaging by nanomechanical photothermal sensing. *Proc Natl Acad Sci U S A.* 2018;115(44):11150–11155. doi:10.1073/pnas.1804174115
92. Zahedian M, Lee Z, Koh ES, Dragnea B. Studies of nanoparticle-assisted photoannealing of polydimethylsiloxane by time-harmonic photothermal microscopy. *ACS Photonics.* 2020;7(9):2601–2609.
93. Boyer D, Tamarat P, Maali A, Lounis B, Orrit M. Photothermal imaging of nanometer-sized metal particles among scatterers. *Science.* 2002;297(5584):1160–1163. doi:10.1126/science.1073765
94. Spaeth P, Adhikari S, Le L, et al. Circular Dichroism measurement of single metal nanoparticles using photothermal imaging. *Nano Lett.* 2019;19(12):8934–8940. doi:10.1021/acs.nanolett.9b03853
95. Shi Z, Tian X, Luo Z, Huang R, Wu L, Li Q. Photothermal imaging of individual nano-objects with large scattering cross sections. *J Phys Chem A.* 2020;124(8):1659–1665. doi:10.1021/acs.jpca.9b11382
96. Li Q, Shi Z, Wu L, Wei H. Resonant scattering-enhanced photothermal microscopy. *Nanoscale.* 2020;12(15):8397–8403. doi:10.1039/C9NR10893A
97. Shokoufi N, Abbasgholi Nejad Asbaghi B, Abbasi-Ahd A. Microfluidic chip-photothermal lens microscopy for DNA hybridization assay using gold nanoparticles. *Anal Bioanal Chem.* 2019;411(23):6119–6128. doi:10.1007/s00216-019-01999-5
98. Mathurin J, Pancani E, Deniset-Besseau A, et al. How to unravel the chemical structure and component localization of individual drug-loaded polymeric nanoparticles by using tapping AFM-IR. *Analyst.* 2018;143(24):5940–5949. doi:10.1039/C8AN01239C
99. Zhang Y, Yurdakul C, Devaux AJ, et al. Vibrational spectroscopic detection of a single virus by mid-infrared photothermal microscopy. *Anal Chem.* 2021;93(8):4100–4107. doi:10.1021/acs.analchem.0c05333
100. Gao H, Wu P, Song P, Kang B, Xu JJ, Chen HY. The video-rate imaging of sub-10 nm plasmonic nanoparticles in a cellular medium free of background scattering. *Chem Sci.* 2021;12(8):3017–3024. doi:10.1039/D0SC04764C
101. Wang G, Li Z, Luo X, Yue R, Shen Y, Ma N. DNA-templated nanoparticle complexes for photothermal imaging and labeling of cancer cells. *Nanoscale.* 2018;10(35):16508–16520. doi:10.1039/C8NR03503B
102. Nedosekin DA, Galanzha EI, Dervishi E, Biris AS, Zharov VP. Super-resolution nonlinear photothermal microscopy. *Small.* 2014;10(1):135–142. doi:10.1002/smll.201300024
103. Bijesh MM, Shakhi PK, Arunkarthick S, Varier GK, Nandakumar P. Confocal imaging of single BaTiO<sub>3</sub> nanoparticles by two-photon photothermal microscopy. *Sci Rep.* 2017;7(1):1643. doi:10.1038/s41598-017-01548-z
104. Darrigues E, Nima ZA, Nedosekin DA, et al. Tracking gold nanorods' interaction with large 3D pancreatic-stromal tumor spheroids by multimodal imaging: fluorescence, photoacoustic, and photothermal microscopies. *Sci Rep.* 2020;10(1):3362. doi:10.1038/s41598-020-59226-6
105. Chang M, Wang M, Shu M, et al. Enhanced photoconversion performance of NdVO<sub>4</sub>/Au nanocrystals for photothermal/photoacoustic imaging guided and near infrared light-triggered anticancer phototherapy. *Acta Biomater.* 2019;99:295–306. doi:10.1016/j.actbio.2019.08.026
106. Flewellen JL, Zaid IM, Berry RM. A multi-mode digital holographic microscope. *Rev Sci Instrum.* 2019;90(2):023705. doi:10.1063/1.5066556
107. Abbasian V, Akhlaghi EA, Charsooghi MA, Bazzar M, Moradi AR. Digital holographic microscopy for 3D surface characterization of polymeric nanocomposites. *Ultramicroscopy.* 2018;185:72–80. doi:10.1016/j.ultramic.2017.11.013
108. Midtvedt B, Olsen E, Eklund F, et al. Fast and accurate nanoparticle characterization using deep-learning-enhanced off-axis holography. *ACS Nano.* 2021;15(2):2240–2250. doi:10.1021/acsnano.0c06902
109. Kim D, Lee S, Lee M, Oh J, Yang SA, Park Y. Holotomography: refractive index as an intrinsic imaging contrast for 3-D label-free live cell imaging. *Adv Exp Med Biol.* 2021;1310:211–238.
110. Leith EN, Upatnieks J. Reconstructed wavefronts and communication theory\*. *J Opt Soc Am.* 1962;52(10):1123–1130. doi:10.1364/JOSA.52.001123

111. Lee SH, Roichman Y, Yi GR, et al. Characterizing and tracking single colloidal particles with video holographic microscopy. *Opt Express*. 2007;15(26):18275–18282. doi:10.1364/OE.15.018275
112. Liebel M, Pazos-Perez N, van Hulst NF, Alvarez-Puebla RA. Surface-enhanced Raman scattering holography. *Nat Nanotechnol*. 2020;15(12):1005–1011. doi:10.1038/s41565-020-0771-9
113. Liebel M, Valduga de Almeida Camargo F, Cerullo G, Hulst N. Widefield phototransient imaging for visualizing 3D motion of resonant particles in scattering environments; 2021.
114. Liebel M, Camargo FVA, Cerullo G, van Hulst NF. Ultrafast transient holographic microscopy. *Nano Lett*. 2021;21(4):1666–1671. doi:10.1021/acs.nanolett.0c04416
115. Kalies S, Antonopoulos GC, Rakoski MS, et al. Investigation of biophysical mechanisms in gold nanoparticle mediated laser manipulation of cells using a multimodal holographic and fluorescence imaging setup. *PLoS One*. 2015;10(4):e0124052. doi:10.1371/journal.pone.0124052
116. Narayanaswamy R, Torchilin VP. Targeted delivery of combination therapeutics using monoclonal antibody 2C5-modified immunoliposomes for cancer therapy. *Pharm Res*. 2021;38(3):429–450. doi:10.1007/s11095-021-02986-1
117. Geloen A, Isaieva K, Isaieva M, Levinson O, Berger E, Lysenko V. Intracellular detection and localization of nanoparticles by refractive index measurement. *Sensors*. 2021;21(15):15. doi:10.3390/s21155001
118. Lemaster JE, Jokerst JV. What is new in nanoparticle-based photoacoustic imaging? *Wiley Interdiscip Rev Nanomed Nanobiotechnol*. 2017;9(1). doi:10.1002/wnan.1404
119. Zhang Y, Hong H, Cai W. Photoacoustic imaging. *Cold Spring Harb Protoc*. 2011;2011(9):pdb.top065508. doi:10.1101/pdb.top065508
120. Park EY, Oh D, Park S, Kim W, Kim C. New contrast agents for photoacoustic imaging and theranostics: recent 5-year overview on phthalocyanine/naphthalocyanine-based nanoparticles. *APL Bioeng*. 2021;5(3):031510. doi:10.1063/5.0047660
121. Ma Y, Xu L, Yin B, et al. Ratiometric semiconducting polymer nanoparticle for reliable photoacoustic imaging of pneumonia-induced vulnerable atherosclerotic plaque in vivo. *Nano Lett*. 2021;21(10):4484–4493. doi:10.1021/acs.nanolett.1c01359
122. Wang Y, Fadhel MN, Hysi E, Pastenak M, Sathiyamoorthy K, Kolios MC. In vivo spectroscopic photoacoustic imaging and laser-induced nanoparticle vaporization for anti-HER2 breast cancer. *J Biophotonics*. 2021;14(10):e202100099. doi:10.1002/jbio.202100099
123. Fu J, Wu Q, Dang Y, et al. Synergistic therapy using doxorubicin-loading and nitric oxide-generating hollow Prussian blue nanoparticles with photoacoustic imaging potential against breast cancer. *Int J Nanomedicine*. 2021;16:6003–6016. doi:10.2147/IJN.S327598
124. St Lorenz A, Buabeng ER, Taratula O, Taratula O, Henary M. Near-infrared heptamethine cyanine dyes for nanoparticle-based photoacoustic imaging and photothermal therapy. *J Med Chem*. 2021;64(12):8798–8805. doi:10.1021/acs.jmedchem.1c00771
125. Wang S, Zhang L, Zhao J, He M, Huang Y, Zhao S. A tumor microenvironment-induced absorption red-shifted polymer nanoparticle for simultaneously activated photoacoustic imaging and photothermal therapy. *Sci Adv*. 2021;7:12.
126. Zhang LP, Kang L, Li X, Liu S, Liu T, Zhao Y. Pyrazino[2,3-g]quinoxaline-based nanoparticles as near-infrared phototheranostic agents for efficient photoacoustic-imaging-guided photothermal therapy. *ACS Appl Nano Mater*. 2021;4(2):2019–2029. doi:10.1021/acsanm.0c03346
127. Ouyang Z, Li D, Xiong Z, et al. Antifouling dendrimer-entrapped copper sulfide nanoparticles enable photoacoustic imaging-guided targeted combination therapy of tumors and tumor metastasis. *ACS Appl Mater Interfaces*. 2021;13(5):6069–6080. doi:10.1021/acsami.0c21620
128. Xu Y, Sun G, Middha E, et al. Organic nanoparticle-doped microdroplets as dual-modality contrast agents for ultrasound microvascular flow and photoacoustic imaging. *Sci Rep*. 2020;10(1):17009. doi:10.1038/s41598-020-72795-w
129. Miao Y, Gu C, Yu B, et al. Conjugated-polymer-based nanoparticles with efficient NIR-II fluorescent, photoacoustic and photothermal performance. *Chembiochem*. 2019;20(21):2793–2799. doi:10.1002/cbic.201900309
130. Li H, Shi S, Wu M, et al. iRGD peptide-mediated liposomal nanoparticles with photoacoustic/ultrasound dual-modality imaging for precision theranostics against hepatocellular carcinoma. *Int J Nanomedicine*. 2021;16:6455–6475. doi:10.2147/IJN.S325891
131. Byrne GD, Pitter MC, Zhang J, Falcone FH, Stolnik S, Somekh MG. Total internal reflection microscopy for live imaging of cellular uptake of sub-micron non-fluorescent particles. *J Microsc*. 2008;231(Pt 1):168–179. doi:10.1111/j.1365-2818.2008.02027.x
132. Prieve DC, Frej NA. Total internal reflection microscopy: a quantitative tool for the measurement of colloidal forces. *Langmuir*. 1990;6(2):396–403. doi:10.1021/la00092a019
133. Temple PA. Total internal reflection microscopy: a surface inspection technique. *Appl Opt*. 1981;20(15):2656–2664. doi:10.1364/AO.20.002656
134. Byrne GD, Vllasaliu D, Falcone FH, Somekh MG, Stolnik S. Live imaging of cellular internalization of single colloidal particle by combined label-free and fluorescence total internal reflection microscopy. *Mol Pharm*. 2015;12(11):3862–3870. doi:10.1021/acs.molpharmaceut.5b00215
135. Chakkarapani SK, Zhang P, Ahn S, Kang SH. Total internal reflection plasmonic scattering-based fluorescence-free nanoimmunosensor probe for ultra-sensitive detection of cancer antigen 125. *Biosens Bioelectron*. 2016;81:23–31. doi:10.1016/j.bios.2016.01.094
136. Braslavsky I, Amit R, Jaffar Ali BM, Gileadi O, Oppenheim A, Stavans J. Objective-type dark-field illumination for scattering from microbeads. *Appl Opt*. 2001;40(31):5650–5657. doi:10.1364/AO.40.005650
137. Nan X, Sims PA, Xie XS. Organelle tracking in a living cell with microsecond time resolution and nanometer spatial precision. *Chemphyschem*. 2008;9(5):707–712. doi:10.1002/cphc.200700839
138. Mickolajczyk KJ, Hancock WO. High-resolution single-molecule kinesin assays at kHz frame rates. *Methods Mol Biol*. 2018;1805:123–138.
139. Ueno H, Nishikawa S, Iino R, et al. Simple dark-field microscopy with nanometer spatial precision and microsecond temporal resolution. *Biophys J*. 2010;98(9):2014–2023. doi:10.1016/j.bpj.2010.01.011
140. Ryu KR, Kim GW, Ha JW. Localized surface plasmon resonance inflection points for improved detection of chemisorption of 1-alkanethiols under total internal reflection scattering microscopy. *Sci Rep*. 2021;11(1):12902. doi:10.1038/s41598-021-92410-w
141. Xia W, Ling B, Wang L, Gao F, Chen H. A near-infrared upconversion luminescence total internal reflection platform for quantitative image analysis. *Chem Commun*. 2020;56(60):8440–8443. doi:10.1039/D0CC03119D
142. Jiang L, Sun X, Liu H, et al. Label-free imaging of single nanoparticles using total internal reflection-based leakage radiation microscopy. *Nanomaterials*. 2020;10(4):615. doi:10.3390/nano10040615
143. Li M, Yuan T, Jiang Y, et al. Total internal reflection-based extinction spectroscopy of single nanoparticles. *Angew Chem Int Ed Engl*. 2019;58(2):572–576. doi:10.1002/anie.201810324
144. Andrén D, Odebo Länk N, Šípová-jungová H, Jones S, Johansson P, Käll M. Surface interactions of gold nanoparticles optically trapped against an interface. *J Phys Chem C*. 2019;123(26):16406–16414. doi:10.1021/acs.jpcc.9b05438

145. Jones S, Andr  n D, Karpinski P, K  ll M. Photothermal heating of plasmonic nanoantennas: influence on trapped particle dynamics and colloid distribution. *ACS Photonics*. 2018;5(7):2878–2887. doi:10.1021/acsp Photonics.8b00231
146. Lal S, Link S, Halas NJ. Nano-optics from sensing to waveguiding. *Nat Photonics*. 2007;1(11):641–648. doi:10.1038/nphoton.2007.223
147. Truong PL, Ma X, Sim SJ. Resonant Rayleigh light scattering of single Au nanoparticles with different sizes and shapes. *Nanoscale*. 2014;6(4):2307–2315. doi:10.1039/c3nr05211g
148. Ringe E, Sharma B, Henry A-I, Marks LD, Van Duyne RP. Single nanoparticle plasmonics. *Phys Chem Chem Phys*. 2013;15(12):4110–4129. doi:10.1039/c3cp44574g
149. Bohren CF, Huffman DR. *Absorption and Scattering of Light by Small Particles*. John Wiley & Sons; 2008.
150. Ma J, Wang X, Feng J, Huang C, Fan Z. Individual plasmonic nanoprobe for biosensing and bioimaging: recent advances and perspectives. *Small*. 2021;17(8):e2004287. doi:10.1002/sml.202004287
151. Lee S, Sun Y, Cao Y, Kang SH. Plasmonic nanostructure-based bioimaging and detection techniques at the single-cell level. *Trends Anal Chem*. 2019;117:58–68. doi:10.1016/j.trac.2019.05.006
152. Shang J, Yang Q, Fan W, et al. Probing dynamic features of phagosome maturation in macrophage using Au@MnOx @SiO2 nanoparticles as pH-sensitive plasmonic nanoprobe. *Chem Asian J*. 2021;16(9):1150–1156. doi:10.1002/asia.202100031
153. Ghotra G, Le NH, Hayder H, Peng C, Chen JIL. Multiplexed and single-cell detection of microRNA with plasmonic nanoparticle assemblies. *Can J Chem*. 2021;99(7):585–593. doi:10.1139/cjc-2021-0023
154. Wang L, Darvot C, Zapata-Farfan J, Patskovsky S, Trudel D, Meunier M. Designable nanoplasmonic biomarkers for direct microscopy cytopathology diagnostics. *J Biophotonics*. 2019;12(11):e201900166. doi:10.1002/jbio.201900166
155. Ge F, Xue J, Wang Z, Xiong B, He Y. Real-time observation of dynamic heterogeneity of gold nanorods on plasma membrane with darkfield microscopy. *Sci China Chem*. 2019;62(8):1072–1081. doi:10.1007/s11426-019-9444-9
156. El-Kurdi R, Patra D. Gold and silver nanoparticles in resonance Rayleigh scattering techniques for chemical sensing and biosensing: a review. *Mikrochim Acta*. 2019;186(10):667. doi:10.1007/s00604-019-3755-4
157. Song MS, Choi SP, Lee J, Kwon YJ, Sim SJ. Real-time, sensitive, and specific detection of promoter-polymerase interactions in gene transcription using a nanoplasmonic sensor. *Adv Mater*. 2013;25(9):1265–1269. doi:10.1002/adma.201203467
158. Truong PL, Choi SP, Sim SJ. Amplification of resonant Rayleigh light scattering response using immunogold colloids for detection of lysozyme. *Small*. 2013;9(20):3485–3492. doi:10.1002/sml.201202638
159. Louit G, Asahi T, Tanaka G, Uwada T, Masuhara H. Spectral and 3-dimensional tracking of single gold nanoparticles in living cells studied by Rayleigh light scattering microscopy. *J Phys Chem C*. 2009;113(27):11766–11772. doi:10.1021/jp9018124
160. Cramer J, Vogt F, Booksh KS. 4.11 - smart sensors. In: Brown SD, Tauler R, Walczak B, editors. *Comprehensive Chemometrics*. Oxford: Elsevier; 2009:357–376.
161. Zamora-Perez P, Tsoutsis D, Xu R, Rivera-Gil P. Hyperspectral-enhanced dark field microscopy for single and collective nanoparticle characterization in biological environments. *Materials*. 2018;11(2):243. doi:10.3390/ma11020243
162. Roth GA, Tahiliani S, Neu-Baker NM, Brenner SA. Hyperspectral microscopy as an analytical tool for nanomaterials. *Wiley Interdiscip Rev Nanomed Nanobiotechnol*. 2015;7(4):565–579. doi:10.1002/wnan.1330
163. Lopez-Luna J, Cruz-Fernandez S, Mills DS, et al. Phytotoxicity and upper localization of Ag@CoFe2O4 nanoparticles in wheat plants. *Environ Sci Pollut Res Int*. 2020;27(2):1923–1940. doi:10.1007/s11356-019-06668-9
164. Th  oret T, Wilkinson KJ. Evaluation of enhanced darkfield microscopy and hyperspectral analysis to analyse the fate of silver nanoparticles in wastewaters. *Analytical Methods*. 2017;9(26):3920–3928. doi:10.1039/C7AY00615B
165. Patskovsky S, Bergeron E, Rioux D, Meunier M. Wide-field hyperspectral 3D imaging of functionalized gold nanoparticles targeting cancer cells by reflected light microscopy. *J Biophotonics*. 2015;8(5):401–407. doi:10.1002/jbio.201400025
166. Roth GA, Sosa Pena Mdel P, Neu-Baker NM, Tahiliani S, Brenner SA. Identification of metal oxide nanoparticles in histological samples by enhanced darkfield microscopy and hyperspectral mapping. *J Vis Exp*. 2015;106:e53317.
167. Liu Y, Naumenko E, Akhatova F, Zou Q, Fakhruddin R, Yan X. Self-assembled peptide nanoparticles for enhanced dark-field hyperspectral imaging at the cellular and invertebrate level. *Chem Eng J*. 2021;424:130348. doi:10.1016/j.cej.2021.130348
168. Nigamatzyanova L, Fakhruddin R. Dark-field hyperspectral microscopy for label-free microplastics and nanoplastics detection and identification in vivo: a *Caenorhabditis elegans* study. *Environ Pollut*. 2021;271:116337. doi:10.1016/j.envpol.2020.116337
169. Pena Mdel P, Gottipati A, Tahiliani S, et al. Hyperspectral imaging of nanoparticles in biological samples: simultaneous visualization and elemental identification. *Microsc Res Tech*. 2016;79(5):349–358. doi:10.1002/jemt.22637
170. Idelchik MPS, Dillon J, Abariute L, et al. Comparison of hyperspectral classification methods for the analysis of cerium oxide nanoparticles in histological and aqueous samples. *J Microsc*. 2018;271(1):69–83. doi:10.1111/jmi.12696
171. Touloumes GJ, Ardon HAM, Casalino EK, et al. Mapping 2D- and 3D-distributions of metal/metal oxide nanoparticles within cleared human ex vivo skin tissues. *NanoImpact*. 2020;17:100208. doi:10.1016/j.impact.2020.100208
172. Zucker RM, Ortenzio J, Degen LL, Lerner JM, Boyes WK. Biophysical comparison of four silver nanoparticles coatings using microscopy, hyperspectral imaging and flow cytometry. *PLoS One*. 2019;14(7):e0219078. doi:10.1371/journal.pone.0219078
173. Persaud I, Shannahan JH, Raghavendra AJ, Alsaleh NB, Podila R, Brown JM. Biocorona formation contributes to silver nanoparticle induced endoplasmic reticulum stress. *Ecotoxicol Environ Saf*. 2019;170:77–86. doi:10.1016/j.ecoenv.2018.11.107
174. Hosseini Z, Alam MN, Sim G, Tufenkji N, van de Ven TG. Cellulose nanocrystals with tunable surface charge for nanomedicine. *Nanoscale*. 2015;7(40):16647–16657. doi:10.1039/C5NR02506K
175. Jenkins SV, Qu H, Mudalige T, et al. Rapid determination of plasmonic nanoparticle agglomeration status in blood. *Biomaterials*. 2015;51:226–237. doi:10.1016/j.biomaterials.2015.01.072
176. Ishmukhametov I, Nigamatzyanova L, Fakhruddin R. Label-free identification of microplastics in human cells: dark-field microscopy and deep learning study. *Anal Bioanal Chem*. 2022;414(3):1297–1312. doi:10.1007/s00216-021-03749-y
177. Neil MA, Juskaitis R, Wilson T. Method of obtaining optical sectioning by using structured light in a conventional microscope. *Opt Lett*. 1997;22(24):1905–1907. doi:10.1364/OL.22.001905
178. Rego EH, Shao L, Macklin JJ, et al. Nonlinear structured-illumination microscopy with a photoswitchable protein reveals cellular structures at 50-nm resolution. *Proc Natl Acad Sci U S A*. 2012;109(3):E135–E143. doi:10.1073/pnas.1107547108



179. Schermelleh L, Carlton PM, Haase S, et al. Subdiffraction multicolor imaging of the nuclear periphery with 3D structured illumination microscopy. *Science*. 2008;320(5881):1332–1336. doi:10.1126/science.1156947
180. Chang BJ, Lin SH, Chou LJ, Chiang SY. Subdiffraction scattered light imaging of gold nanoparticles using structured illumination. *Opt Lett*. 2011;36(24):4773–4775. doi:10.1364/OL.36.004773
181. Guggenheim EJ, Khan A, Pike J, Chang L, Lynch I, Rappoport JZ. Comparison of confocal and super-resolution reflectance imaging of metal oxide nanoparticles. *PLoS One*. 2016;11(10):e0159980. doi:10.1371/journal.pone.0159980
182. Guggenheim EJ, Rappoport JZ, Lynch I. Mechanisms for cellular uptake of nanosized clinical MRI contrast agents. *Nanotoxicology*. 2020;14(4):504–532. doi:10.1080/17435390.2019.1698779
183. Aslam N, Pfender M, Neumann P, et al. Nanoscale nuclear magnetic resonance with chemical resolution. *Science*. 2017;357(6346):67–71. doi:10.1126/science.aam8697
184. Boss JM, Cujia KS, Zopes J, Degen CL. Quantum sensing with arbitrary frequency resolution. *Science*. 2017;356(6340):837–840. doi:10.1126/science.aam7009
185. Degen CL, Reinhard F, Cappellaro P. Quantum sensing. *Rev Mod Phys*. 2017;89(3):035002. doi:10.1103/RevModPhys.89.035002
186. Nagy R, Dasari DBR, Babin C, et al. Narrow inhomogeneous distribution of spin-active emitters in silicon carbide. *Appl Phys Lett*. 2021;118(14):144003. doi:10.1063/5.0046563
187. Schmitt S, Gefen T, Stürner FM, et al. Submillihertz magnetic spectroscopy performed with a nanoscale quantum sensor. *Science*. 2017;356(6340):832–837. doi:10.1126/science.aam5532
188. Taylor JM, Cappellaro P, Childress L, et al. High-sensitivity diamond magnetometer with nanoscale resolution. *Nat Phys*. 2008;4(10):810–816. doi:10.1038/nphys1075
189. Doherty MW, Struzhkin VV, Simpson DA, et al. Electronic properties and metrology applications of the diamond NV-center under pressure. *Phys Rev Lett*. 2014;112(4):047601. doi:10.1103/PhysRevLett.112.047601
190. Dolde F, Fedder H, Doherty MW, et al. Electric-field sensing using single diamond spins. *Nat Phys*. 2011;7(6):459–463. doi:10.1038/nphys1969
191. Kucsko G, Maurer PC, Yao NY, et al. Nanometre-scale thermometry in a living cell. *Nature*. 2013;500(7460):54–58. doi:10.1038/nature12373
192. Neumann P, Jakobi I, Dolde F, et al. High-precision nanoscale temperature sensing using single defects in diamond. *Nano Lett*. 2013;13(6):2738–2742. doi:10.1021/nl401216y
193. Wolf T, Neumann P, Nakamura K, et al. Subpicotesla diamond magnetometry. *Physical Review X*. 2015;5(4):041001. doi:10.1103/PhysRevX.5.041001
194. Barbiero M, Castelletto S, Zhang Q, et al. Nanoscale magnetic imaging enabled by nitrogen vacancy centres in nanodiamonds labelled by iron-oxide nanoparticles. *Nanoscale*. 2020;12(16):8847–8857. doi:10.1039/C9NR10701K
195. Murray RA, Escobar A, Bastús NG, Andreozzi P, Puentes V, Moya SE. Fluorescently labelled nanomaterials in nanosafety research: practical advice to avoid artefacts and trace unbound dye. *NanoImpact*. 2018;9:102–113. doi:10.1016/j.impact.2017.11.001
196. Alamo P, Pallares V, Cespedes MV, et al. Fluorescent dye labeling changes the biodistribution of tumor-targeted nanoparticles. *Pharmaceutics*. 2020;12(11):11. doi:10.3390/pharmaceutics12111004

International Journal of Nanomedicine

Dovepress

## Publish your work in this journal

The International Journal of Nanomedicine is an international, peer-reviewed journal focusing on the application of nanotechnology in diagnostics, therapeutics, and drug delivery systems throughout the biomedical field. This journal is indexed on PubMed Central, MedLine, CAS, SciSearch®, Current Contents®/Clinical Medicine, Journal Citation Reports/Science Edition, EMBase, Scopus and the Elsevier Bibliographic databases. The manuscript management system is completely online and includes a very quick and fair peer-review system, which is all easy to use. Visit <http://www.dovepress.com/testimonials.php> to read real quotes from published authors.

Submit your manuscript here: <https://www.dovepress.com/international-journal-of-nanomedicine-journal>